



**Marie Curie Initial Training Network
Environmental Chemoinformatics (ECO)**

Final Report

31 July 2013

**Polymer and Polymer Degradation Products in
Aqueous Environment**

Early stage researcher:

Ian Ken D. Dimzon

Project supervisor:

Thomas P. Knepper

Research Institution:

Institute for Analytical Research

ECO Final Report Acknowledgement

I would like to extend my heartfelt gratitude to the European Commission for funding the Initial Training Network Project called Environmental Chemoinformatics (ECO-ITN).

I thank Prof. Dr. Thomas P. Knepper for putting his trust on me and allowing me to work as the Hochschule Fresenius' (HSF) long term Marie Curie Fellow. I appreciate the hospitality as well as the very good training I have in the institute.

I thank Mrs. Heike Weil for her support and assistance, especially in the most difficult times.

I thank Dr. Eva Schlosser for her understanding and patience with us.

I thank my colleagues at the HSF: Jutta Müller, Tobias Frömel, Marco Bernhard and Sascha Klein for the technical help that they have extended during the long hours of laboratory works.

I thank Dr. Pim de Voogt for accepting the role of being my first supervisor for my doctoral works at the University of Amsterdam.

I thank my mentees and friends who had worked with me: Chiragkumar Patel and Mohammad Javanmardi.

I thank the companies Chemetall and Certmedica for collaborating with us.

I thank most especially my family and friends who have been and will always be with me in this journey.

August 2010 – July 2013

Polymers and Polymer Degradation Products in Aqueous Environment

I. Introduction

Polymers are composed of repeating structural units called monomers. A polymer can be made-up of one (homopolymer) or more (copolymer) type of monomers linked together by a covalent bond. The European Chemicals Agency (ECHA) specifies that a polymer is a “sequence of at least three monomer units” bound to “at least one other monomer unit or other reactant” [1]. The degree of polymerization (DP) refers to the total number of basic structural units including the end group. DP is related to both the chain length and to the molecular weight [2]. Polymers are usually distributed over a range of molecular weights. The polydispersity index, calculated as the ratio of the weight average molecular weight (M_w) to the number average molecular weight (M_n), describes the size distribution of the polymer. Polymers vary in the way one or more monomer units are arranged in a microstructure. They can be linear, branched or cyclic. Many polymers are functionalized in the monomers or in the end group to enhance their properties.

By varying the monomer composition, average size, distribution, microstructure and the functional groups attached to the monomer, materials scientists and engineers are able to synthesize thousands of different polymer substances with a wide range of physico-chemical properties to suit a variety of uses. Indeed, many of the things being used today - from pharmaceuticals, cosmetics and household items; to construction and building supplies; to packaging and electronics contain polymer components.

Polymers are exempted from registration and evaluation under the European Registration, Evaluation, Authorization and Restriction of Chemicals (REACH) framework [3]. Compared to other substances, the risk posed by polymers is minimal due to their high molecular weight [1]. Specific polymers may however be subject to authorization and restriction after evaluation of the risk they pose to human health and to the environment. On the other hand, monomers and intermediates are not exempted from registration and evaluation. In relation to the policy, there is a need to differentiate in a polymer sample the individual molecular specie, including the unreacted monomer impurities.

Because of their wide range of applications, polymers have become ubiquitous in the environment. Soluble, polar polymers readily enter the aqueous environment as part of effluents. Many of the synthetic polymers degrade very slowly making them proliferate in the ecosystems. Researches on the fate and degradation of polymers are necessary to better understand the long-term effects of these compounds in the environment. A highly selective but more robust and sensitive analytical method is indispensable to understand the transformations of these substances during the degradation process.

A number of techniques are currently used to characterize polymers. Infrared (IR), raman, UV-visible and nuclear magnetic resonance (NMR) spectroscopy are used to determine and confirm monomer composition and degree of functionalization. Gel permeation chromatography (GPC) with refractive index, viscosity and light scattering detectors is used to estimate the average molecular weight and the polydispersity index. These techniques along with others like x-ray crystallography, differential scanning calorimetry, and dynamic mechanical analysis are used to test the physico-chemical properties of the raw or bulk polymers. These techniques, however, may not be fit-for-purpose in other areas of polymer research like in the structure elucidation of the individual components and in structure-property-activity relationship studies.

The use of mass spectrometry (MS) in polymer analysis has greatly increased at the onset of the 21st century. This trend was primarily driven by the development in the soft-ionization techniques like matrix-assisted laser desorption ionization (MALDI) and electrospray ionization (ESI) and by the improvements in the time-of-flight (TOF) mass analyzers. MS is not regarded as an alternative to the existing methods of polymer characterization but rather a complimentary method that gives additional information about the structure, absolute molecular weights, and degree of polymerization and functionalization, and end groups of the polymer. In contrast to NMR that is a widely used method to gain insight on the monomer composition and the general polymer structure, MS provides information on the identity and the relative amounts of every component present in a polymer sample including unreacted monomers.

MS offers a fast, robust, highly selective and sensitive method of detecting polymers. The capabilities of MS can be exploited to widen the scope of polymer analysis beyond the realm of materials science to other areas like environmental science, pollution control and sustainable development. Currently, the use of MS in polymer research is limited by the molecular weight of the polymer under study and the diversity and complexity of polymer mixtures. These limitations are addressed by careful selection of a better suited MS and sample preparation techniques.

The unique tandem of MALDI and TOF is of particular interest as it has become one of the routine [4] but most powerful tools in polymer analysis today.

With the advent of fast computers, the use of statistics and informatics in all fields of science has also dramatically increased. In the area of analytical chemistry, chemometrics is rapidly becoming popular. Chemometrics makes use of “mathematical, statistical and other methods of logic to determine (often by indirect means) the properties of substances” [5]. Multivariate chemometric techniques make possible the characterization of difficult-to-analyze compounds and complex mixtures using data from simple instrumental techniques like spectroscopy. Partial least squares (PLS) is one of the basic and commonly used tool of chemometrics [6].

The general objective of this work was to develop and use multi-technique but polymer-specific methods to polymer characterization. Given the diversity in polymeric composition and structure (monomer/s used; the number, distribution and type of linkage of monomers per molecule; and the side chains and end groups attached), traditional single-technique approaches to characterization are often limited and inadequate, especially to polar synthetic polymers. The work can be divided into three parts according to the polymer used. Each part had its own specific objectives. These specific objectives are introduced in the sections devoted to specific polymers of this report.

Three very different polymers were investigated: Chitosan and chitosan oligosaccharides (COS), 1-aminopropyl oligosiloxanes and polyethylene glycol. Classical techniques like chromatography and spectroscopy were used in complimentary with the more modern ones like mass spectrometry and chemometrics to get a more accurate overview of the polymer molecular weight distribution and composition.

II. Chitosan and COS

Chitosan has been widely used for a variety of purposes. Commercially available chitosan is mainly obtained from chitin, an abundant carbohydrate polymer [7, 8]. Chitin is composed mainly of N-acetyl-D-glucosamine monomer units and the rest are D-glucosamine monomers linked by β -D-(1 \rightarrow 4) glycoside bonds. Alkali-catalyzed deacetylation of N-acetyl-D-glucosamine in chitin leads to the formation of more glucosamine monomers. The extent of this reaction of chitin is described by the property degree of deacetylation (DD). DD is the ratio

(usually expressed in percent) of the amount (in moles) of D-glucosamine units to the total D-glucosamine and N-acetyl-D-glucosamine units. Chitosan is formed when the DD reaches a certain value [9]. For example, chitosan contains a minimum of 60% D-glucosamine units [10].

Chitosan is a mixture of homologues at a wide range of degree of polymerization (DP) and molecular weight (MW). A GPC method that uses neutral stationary phase and a high ionic strength, acidic mobile phase was shown to be robust for the determination of the molecular weight of chitosan [11].

Both the DD and DP are basic physico-chemical properties on which the other properties of chitosan depend. For example, the DP and DD influence the viscosity of chitosan solutions. The Mark – Houwink equation (equation 1) shows that the intrinsic viscosity ($[\eta]$) of a polymer solution changes with the molecular weight. A study by [12]Wang et al. showed that for chitosan samples of the same DD, the logarithm of intrinsic viscosity is a linear function of the logarithm of M_w , consequently is directly proportional to the logarithm of DP. On the other hand, DD influenced the Mark – Houwink constants k and α [12] and the non-Newtonian flow properties of chitosan solutions [13].

$$[\eta] = k M^\alpha \quad \text{Equation 1}$$

DD and DP also influence chitosan solubility in aqueous solutions. Chitosan solubility in water increases with the decrease in the DP and with the increase in DD. The ability of the amine group to gain a positive charge in acidic environment makes the deacetylated chitosan easily dissolve in aqueous acidic medium [14-16]. It was also reported that chitosan behaviors in aqueous solutions of high ionic strength like refractive index and gyration radius are functions of DD. The interactions of chitosan in aqueous solutions can be divided into three domains based on the DD: 1) at $DD > 80\%$, electrostatic interaction predominates; 2) at $50\% < DD < 80\%$, hydrophobic and hydrophilic interactions are counter balanced; and 3) at $DD < 50\%$, stable aggregates are favored [17]. Additionally, chitosan in dilute aqueous solutions has a semi-flexible rod conformation [18]. The rigidity in the structure of chitosan and chitin is mainly due to the interchain H bonds [19].

One of the recent uses of chitosan is as an active ingredient in “fat-binder” tablets or anti-obesity supplements [20]. It is claimed that chitosan has the ability to “bind” with fatty substances in the

intestines making them unavailable for metabolism and they are consequently excreted. Many studies substantiate these claims. *In vivo* studies show that chitosan has hypocholesterolemic effect in humans [21, 22] and in other animal subjects such as mice or rats [21, 23, 24]. Chitosan was also associated with the increase in fecal fat [23, 25-28] and fecal bile acid [23] excretion. *In vitro* studies, on the other hand, reveal that the interaction of chitosan with triacylglycerides contained in olive oil, is highly influenced by the physico-chemical properties of the former. These studies rely mainly on measuring the oil-binding capacity (called fat-binding capacity in some papers) of chitosan. In the test, olive oil is made to form a stable complex with a test substance under a simulated gastrointestinal condition [29]. The unbound oil is separated from the stable complex and is measured. The difference between the initial amount of oil added and the measured amount of unbound oil gives the amount of the oil bound to the complex and is taken as a measure of the oil-binding capacity [30]. It was shown that the oil-binding capacity of chitosan is negatively related to its bulk density and is directly related to viscosity [30]. It was also shown that for a series of chitosan with increasing MW but constant DD, highest oil binding was achieved in an optimal MW [31]. Despite the efforts, however, only a number of significant correlations have been demonstrated [7]. This can be due to the fact that the mechanism of interaction of triacylglyceride and chitosan is a complex process.

In this section, it is shown how to characterize chitosan using multi-technique approach. This section is divided into three parts: A. Determination of the degree of deacetylation of chitosan by infrared spectroscopy and partial least squares; B. Determination of the molecular weight distribution of chitosan and COS by GPC, MALDI-MS and ESI-MS; C. Interaction of chitosan with olive oil. Part C is an application of parts A and B.

A. Determination of the degree of deacetylation of chitosan

It is shown above how the properties of chitosan are dependent on its DD and MW. There are many ways to determine the DD but perhaps the most practical and easiest one is to do an IR analysis of the solid samples in KBr pellets. IR have also many limitations that narrows its scope of application. For one, water present as an impurity contributions to additional absorptions for hydroxyl group at 3020 cm^{-1} . Intra- and inter- molecular hydrogen bonds shifts the absorption maxima of the amide signals. In this study, the IR determination is improved with chemometrics data processing.

Chitosan samples S1 to S10 were pure chitosan samples with corresponding COA. The COA specified the DD of the polymers. There was no need for an additional experiment to determine the DD of these samples. The DD values are summarized in Table 1. Chitosans S1 to S10 were also used as calibration standards to determine the DD of U1 and U2 with FT-IR in combination with PLS chemometric technique. Traditionally, in determining the DD using FT-IR, the absorbances of chitosan standards with known DD at two wavenumbers are selected. One is the characteristic wavenumber which is related to the amide vibrations and can be correlated to the number of the N-acetyl-D-glucosamine monomers. The other is the reference wavenumber which is usually related to the hydroxyl groups or the bridge oxygen – carbon bond in the main pyranose ring and can be correlated to the total number of N-acetyl-D-glucosamine and D-glucosamine monomers. The absorbance ratio of the characteristic wavenumber to the reference wavenumber is plotted against DD generating an inverse linear calibration curve that can be used to determine the DD of an unknown chitosan [32, 33].

An alternative method is to consider the whole amide absorption band and correlate the changes in its shape with the change in DD. Figure 1 shows how the infrared absorption band shape in the wavenumber region 1800 to 1500 cm^{-1} varies with DD. The absorption at approximately 1660 cm^{-1} is due to the amide I bond vibrations (C=O stretching). Only the N-acetyl-D-glucosamine monomers will exhibit the absorption, thus, as DD is increased, the absorption at this wavenumber is decreased relative to the neighboring band. This creates a change in the shape of the normalized bands. By visual inspection, one can easily deduce that the U2 has almost the same shape as the chitosan with DD of 84.7 %.

Table 1. DD of the chitosan samples. Data for S1 to S10 were directly lifted from the COA while for U1 and U2 were obtained experimentally using FT-IR and PLS.

| Sample Code | DD (%) |
|-------------|--------|
| S1 | 94.3 |
| S2 | 73.6 |
| S3 | 91.8 |
| S4 | 89.7 |
| S5 | 84.7 |
| S6 | 94.2 |
| S7 | 78.1 |
| S8 | 89.4 |
| S9 | 93.4 |
| S10 | 92.7 |
| U1 | 83.8 |
| U2 | 82.2 |

The PLS method provides a way of estimating more accurately the DD of the unknown samples. PLS was specifically chosen from a number of other multivariate regression techniques like the component regression (PCR) because of its robustness to factors with high variance but not at all correlated to the dependent property [34, 35]. In this chemometric technique, the absorptions of the individual wavenumber within the infrared spectral region $1800 - 1500 \text{ cm}^{-1}$ are taken as unique variables. Through the algorithm specified in the PLS package for R (the default Kernel algorithm was used [34]), the number of original variables are reduced to only a few components (latent variables) . Features reduction is done by linear combination of the original variables [36]. Characteristic of any algorithm used in this family of techniques, the first component is always chosen so that it explains the greatest variation in the spread of data points, component 2 explains the 2nd greatest variation and so on. Ideally, in the end all the components should be able to explain 100% of the variations in the data. One or more of these components can be used to generate the 'scores' that have a linear relationship with the property being predicted, thus can be used as x-variables in a regression model.

In the analysis, the 'pls' function generated a PLS model with 8 components. To find out which of the 8 components or their combinations have a linear relationship with DD, model validation was simultaneously performed using the LOO validation technique. In LOO, one sample is taken out and the model is generated using the remaining samples. The one taken out is then

used as a test sample. This process is repeated until a substantial amount of validation points are gathered. The predicted values of the validation points are then compared to the experimental or labeled values. The RMSEP can be calculated based on the difference between the predicted and experimental values. In this study, results revealed that if only the first component was taken into account in the prediction, the RMSEP was 2.35 %. This value was lowered to 1.81 % if the first and second components were taken. The value was increased again if the rest of the components were added. This implies that two is the optimum number of components in the regression to predict DD. Figure 2 shows the external validation using the PLS model with only two components. The low deviation from the dotted line (representing values in the COA = PLS-predicted values) is consistent with the computed RMSEP of 1.78 %. The model was thus used to predict the DD of U1 and U2. The results gave 83.8% and 82.2% DD for U1 and U2 respectively (also shown in Table 1). The relative standard deviation was below 3% for the two to four trial runs.

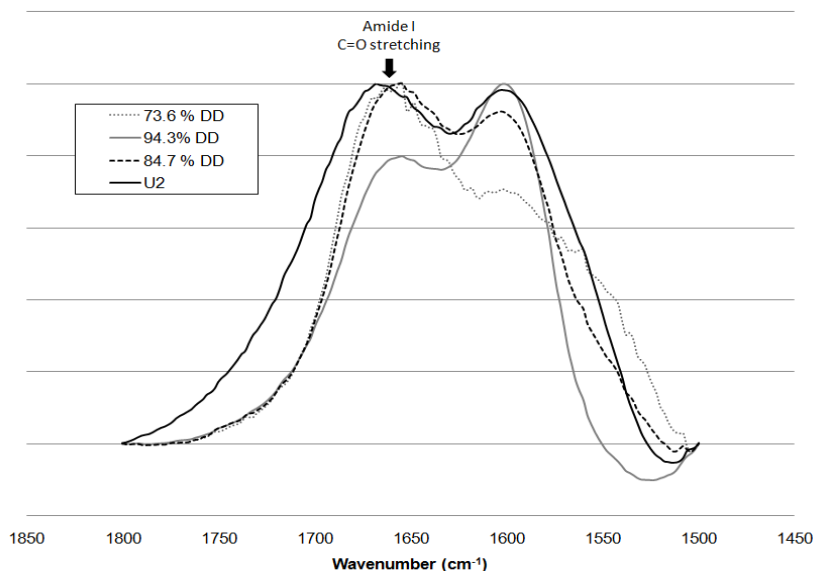


Figure 1. FT-IR absorption spectra (normalized to relative to the highest absorbance) at the wavenumber region 1800 to 1500 cm^{-1} of chitosan samples with known DD (73.6%, 94.3% and 84.7%) and of a chitosan sample with unknown DD (U1). The spectra were corrected for the baseline drawn from 1800 to 1500 cm^{-1} .

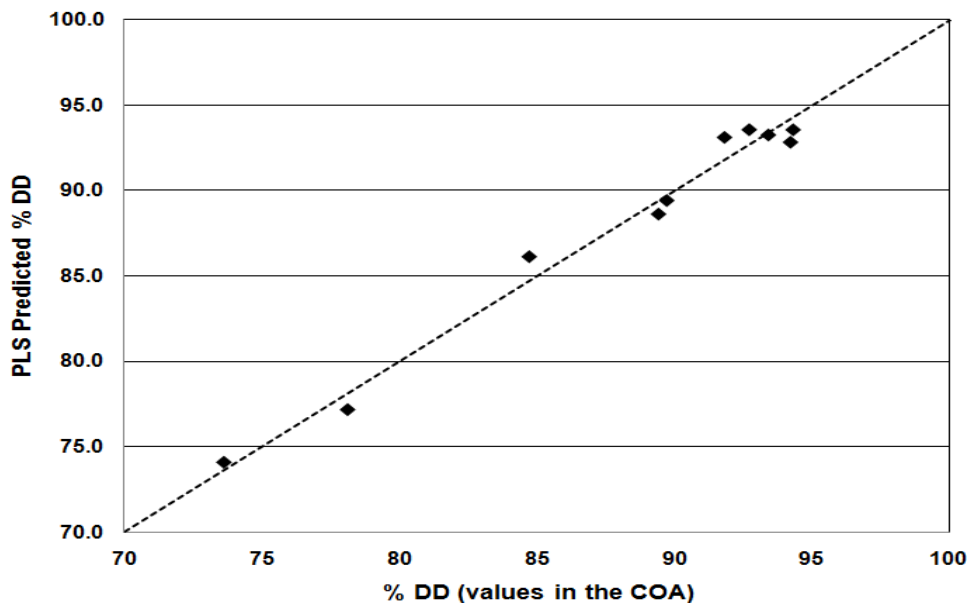


Figure 2. External validation of the PLS model to predict the DD of chitosan. The dotted line represents: DD values in the COA = PLS-predicted DD values.

B. Molecular weight distribution of chitosan and COS

MW is also an important property. The MW differences result from the differences in the degree of polymerization (DP) and DD. The polydispersity index (PDI) would also play a major role in explaining some properties of chitosan. It is discussed earlier that the main challenge in GPC is if the MW standards used are not the same polymer as the samples being analyzed. There is no chitosan MW standard available and so the underlying problem is to develop a rugged GPC method that makes use of poly (2-vinylpyridine) as the MW standard. The researcher did only one part of the experiment in the method development and thus only that part is discussed in the next paragraphs.

GPC was used to estimate the MW and DP of chitosan. Most of the chitosan samples are only partially soluble in the mobile phase used. It was thus necessary to use another solvent system to dissolve the chitosan with. The researcher's part in this project was to compare the molecular weight obtained if a new solvent is used. To accomplish this, chitosans S1 and U1 were dissolved in two solvent systems: 0.5% (v/v) TFA, 0.3 mol·L⁻¹ NaCl in Milli-Q water and 0.2 mol·L⁻¹ acetic acid with 0.1 mol·L⁻¹ sodium acetate in Milli-Q water. The solubility of the chitosan samples in the two solvent systems was the primary consideration in using them. Figure 3 shows the comparison of the M_n , M_w and M_p obtained for the chitosan samples dissolved in the

two solvent systems. It can be observed that there are some differences in the M_n , M_w and M_p of the samples when dissolved in different solvent systems. The percent difference in the molecular weights of the chitosan samples in the two solvent systems was minimal in M_w (<5%) and large in M_n , M_p and D (13 – 22 %).

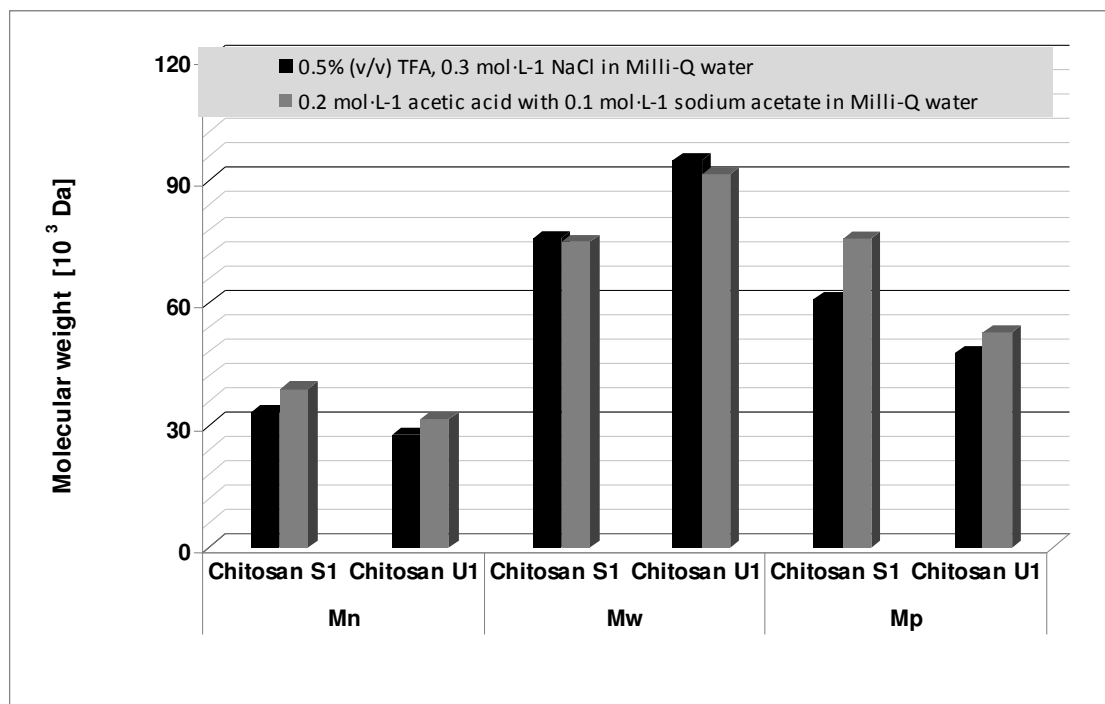


Figure 3. Comparison of the M_n , M_w and M_p of Chitosans S1 and U1 dissolved in 0.5% (v/v) TFA, 0.3 mol·L⁻¹ NaCl in Milli-Q water and in 0.2 mol·L⁻¹ acetic acid with 0.1 mol·L⁻¹ sodium acetate in Milli-Q water ($n = 3$, all RSDs < 5%).

Two-tailed student's t-test was performed to determine if the observed differences are significantly different. Table 2 shows the p-values derived when the M_n , M_w , M_p and D are compared for the samples dissolved in 0.5% (v/v) TFA, 0.3 mol·L⁻¹ NaCl in Milli-Q water and 0.2 mol·L⁻¹ acetic acid with 0.1 mol·L⁻¹ sodium acetate in Milli-Q water. At 95% confidence ($p = 5\%$), M_n , M_p and D are significantly different while M_w is constant. The significant decrease in D of chitosan dissolved in acetate buffer is brought about by the increase in the M_n .

The solvent system where the chitosan is dissolved, affects the later's hydrodynamic volume in the solution. At the start of the GPC run, chitosan has different hydrodynamic volumes in the different solvent systems. However, as the elution in the GPC stationary phase progress, the

chitosan molecules are separated from the other components of the solvent system and the mobile phase becomes its new environment. Since the mobile phase is the same, the difference brought about by the difference in the solvent system is partially minimized during the process.

Table 2. Derived p-values when the M_n , M_w , M_p and D are compared for the samples dissolved in 0.5% (v/v) TFA, 0.3 mol·L⁻¹ NaCl in Milli-Q water and in 0.2 mol·L⁻¹ acetic acid with 0.1 mol·L⁻¹ sodium acetate in Milli-Q water are compared using two-tailed Student's t-test (n = 3).

| Parameter | Chitosan S1 | Chitosan U1 |
|-----------|-------------|-------------|
| M_n | 0.6 | 1.3 |
| M_w | 19.3 | 48.7 |
| M_p | 0.0 | 1.9 |
| D | 0.2 | 0.1 |

The use of 0.3 M acetate buffer as a solvent system for chitosan was shown to give an M_w that is not statistically different from the M_w if the mobile phase 0.2% TFA in 0.3 M NaCl in Milli-Q water is used [5]. From the M_w and DD data, the DP_w of S1 to S10 was calculated using Equation 1. The calculated DP_w of the samples are summarized in Table 3.

Table 3. DP_w of the chitosan samples.

| Sample Code | DP_w |
|-------------|--------|
| S1 | 474 |
| S2 | 589 |
| S3 | 583 |
| S4 | 802 |
| S5 | 905 |
| S6 | 912 |
| S7 | 1076 |
| S8 | 987 |
| S9 | 1063 |
| S10 | 1440 |
| U1 | 542 |
| U2 | 539 |

In an ideal case, MALDI-MS and ESI MS are two techniques that can be used to confirm the molecular weight distribution obtained using GPC. However, up to this time, MS of larger molecular weight chitosan remains an analytical challenge. This can be due to polycationic nature of chitosan under some conditions. Fortunately, low molecular weight COS are

detectable in the MS. COS therefore was used to compare the results obtained by GPC to the results obtained by MALDI and ESI MS.

All MALDI-TOF MS analysis of COS was carried out using Briflex™ III Bruker Daltonics MALDI-TOF-MS with a nitrogen laser emitting at 337 nm in a reflector mode and pulsed at 3 ns. The signals monitored were from positive ions at the $0 \leq m/z \leq 3000$ range. Otherwise stated, the spectra shown were the sum of 300 shots (10 points x 30 shots/point) at 20-40 % laser attenuation. The instrument was externally calibrated using the generated mass spectrum of polyethylene glycol standard ($M_p = 1000$) at 26% laser attenuation

The initial step done was to determine the appropriate matrix to use. In the case of COS, 2,5-DHB was often used matrix in a number of studies involving oligosaccharides. Preliminary experiments, done in-house, showed that COS was ionized better with 2,5-DHB than with other matrices like dithranol, sinapinic acid (SA), 4-HCCA, 2,4,6-Trihydroxyacetophenone (THAP) and trans-2-[3-(4-tert-Butylphenyl)-2-methyl-2-propenylidene]malononitrile (DCTB). Of the matrices tested, only 2,5-DHB, THAP and DCTB were completely soluble in methanol. THAP and 2,5-DHB were able to ionize COS. Eventually, 2,5-DHB was preferred than THAP as the matrix for COS in the proceeding steps because it gave more intense analyte ions.

The second step done was to determine an appropriate sample preparation technique and solvent system. The MALDI sample was prepared on the target using three different techniques: dried droplet, quick and dirty and vacuum drying. Two solvent systems, namely 1:1 methanol : water (MeOH : H₂O) and 1:5 acetonitrile : water (ACN : H₂O) were tested.

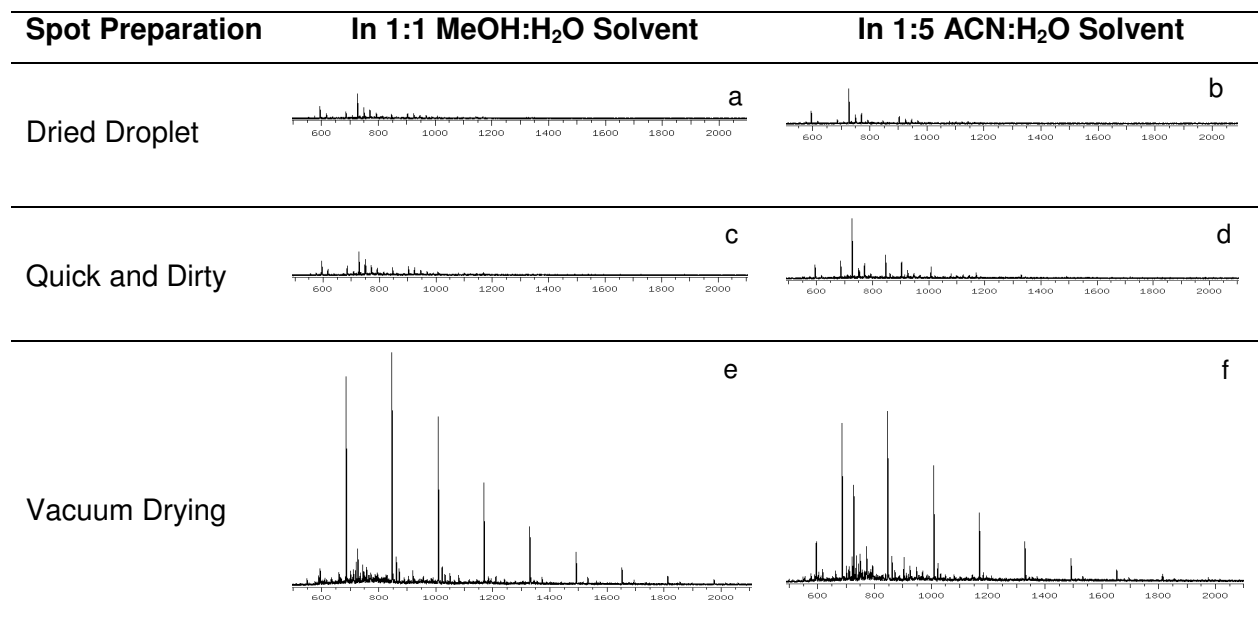


Figure 4. Comparison of MALDI-TOF Spectra (positive mode) obtained using different spot preparation techniques

To compare the intensity of the analyte signals produced from the different sample spots, the laser is beamed on 10 random points in the spots. At each point, the laser shot 30 times. The resulting spectrum generated was the sum of 300 shots. Figure 4 shows the generated mass spectra of the sample prepared using the different spot preparation techniques. Vacuum dried sample spots (Figure 4e and 4f) produced the most intense analyte signals (more than 10 times greater than from the other sample spots). Because of the random nature of spectra generation, less analyte signals were observed from the other samples. As explained earlier, locating the hot spots is very important in dried droplet and in quick and dirty methods. The spectra from sample prepared by dried droplet and quick and dirty were dominated by matrix signals.

Vacuum drying technique produced a mixture of COS and DHB that is evenly spread within the whole diameter of the sample spot. These are the characteristics of ideal MALDI spots. On the other hand, the other techniques produced unevenly spread spots with large crystals accumulating at the periphery of the spot. As a consequence, vacuum dried spots gave better MALDI MS spectrum: matrix signals were low relative to analyte signals and higher molecular weight analytes were also detected with high accuracy.

Shown in Figure 5 is the MALDI-TOF spectrum (positive mode) of COS mixed with DHB matrix in 1:5 ACN : H₂O and prepared by vacuum drying. The ions with most intense signal

detected were that of the sodium adducts of COS. The sodium ions came from the 0.15 M sodium chloride (NaCl) solution intentionally added as cationization agent. The lowest mass that can be attributed to the oligosaccharide is the m/z 686 Da (sodium adduct of the oligosaccharide with 4 chitosan monomer units). The m/z difference of 161 Da is the mass of a deacetylated chitosan monomer. The mass differences between the experimental and the corresponding theoretical values were all less than 0.08% (800 ppm).

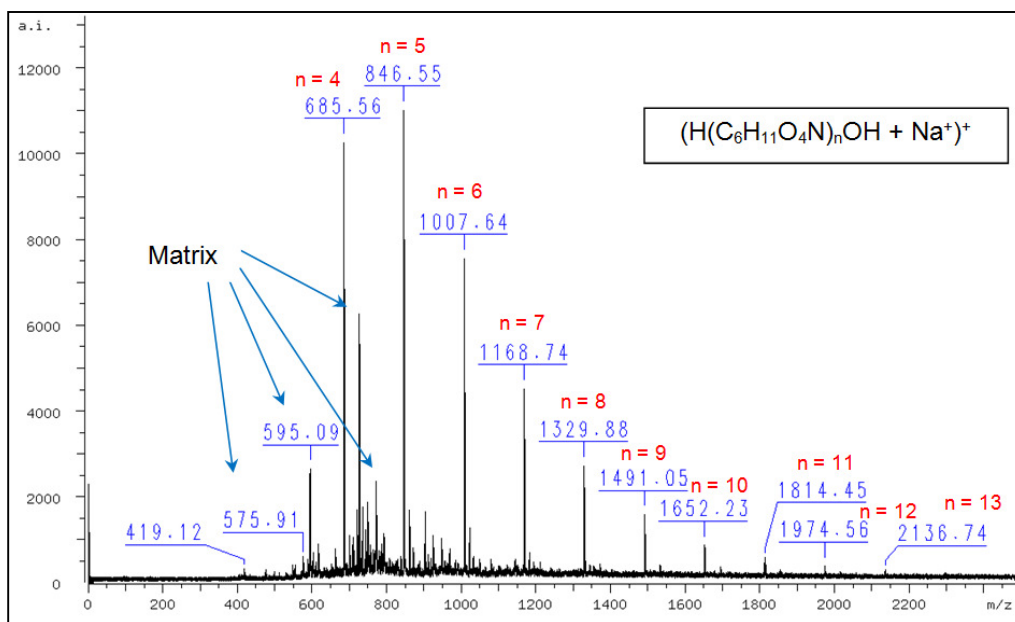


Figure 5. MALDI-TOF Spectrum (positive mode) of COS with 2,5-DHB matrix prepared by vacuum drying.

A parallel GPC run was done to determine the average molecular weight and polydispersity of the COS sample. Separation was done in Novema 100 and Novema 1000 dual column with aqueous 0.3 M NaCl, 0.2% trifluoroacetic acid as mobile phase. The flow rate was maintained at 1.0 ml/min. Figure 6 shows the generated chromatogram and the summary of average molecular weights derived using polyvinyl pyridine standards.

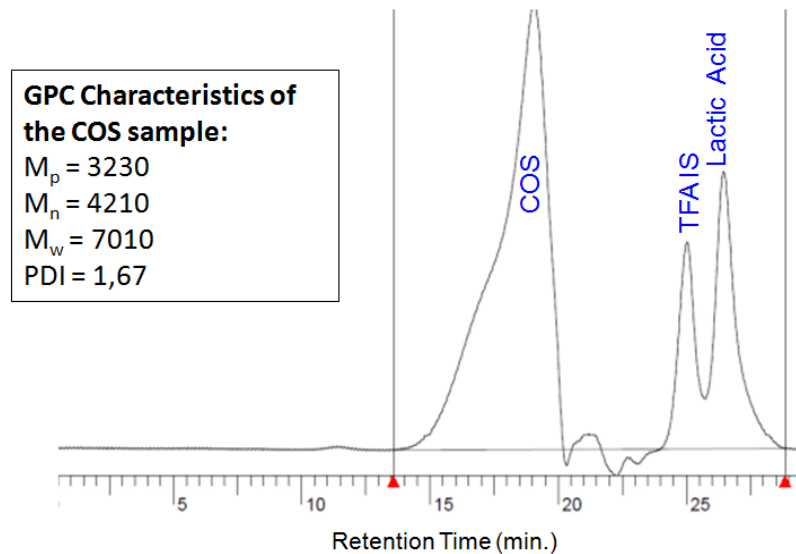


Figure 6. Gel permeation chromatogram of COS in Novema 100 and Novema 1000 dual column with aqueous 0.3 M NaCl, 0.2% trifluoroacetic acid as mobile phase

The obtained peak-average molecular weight (M_p) value (3230 Da) from GPC was way too high compared to the modal molecular weight (M_m) value (846 Da) in the mass spectrum. This can be attributed to the nature of the method used for the determination of molecular weight. In GPC, the limitation was the use of a standard which is different in structure from the COS. In the MALDI-TOF MS, the bias against high molecular weight COS was not yet fully studied.

To further verify the distribution of the COS, fractions were collected corresponding to the the GPC peak and were analyzed in the MALDI-TOF. Figure 7 shows the generated MALDI spectra of the fractions collected from retention time 18.0 to 20.0 minutes. The spectrum with most intense signals was generated from the fraction at 19.5-20.0 min (Figure 7d). The M_m is 846 Da that also corresponds to the M_m of the COS solution (not fractionated).

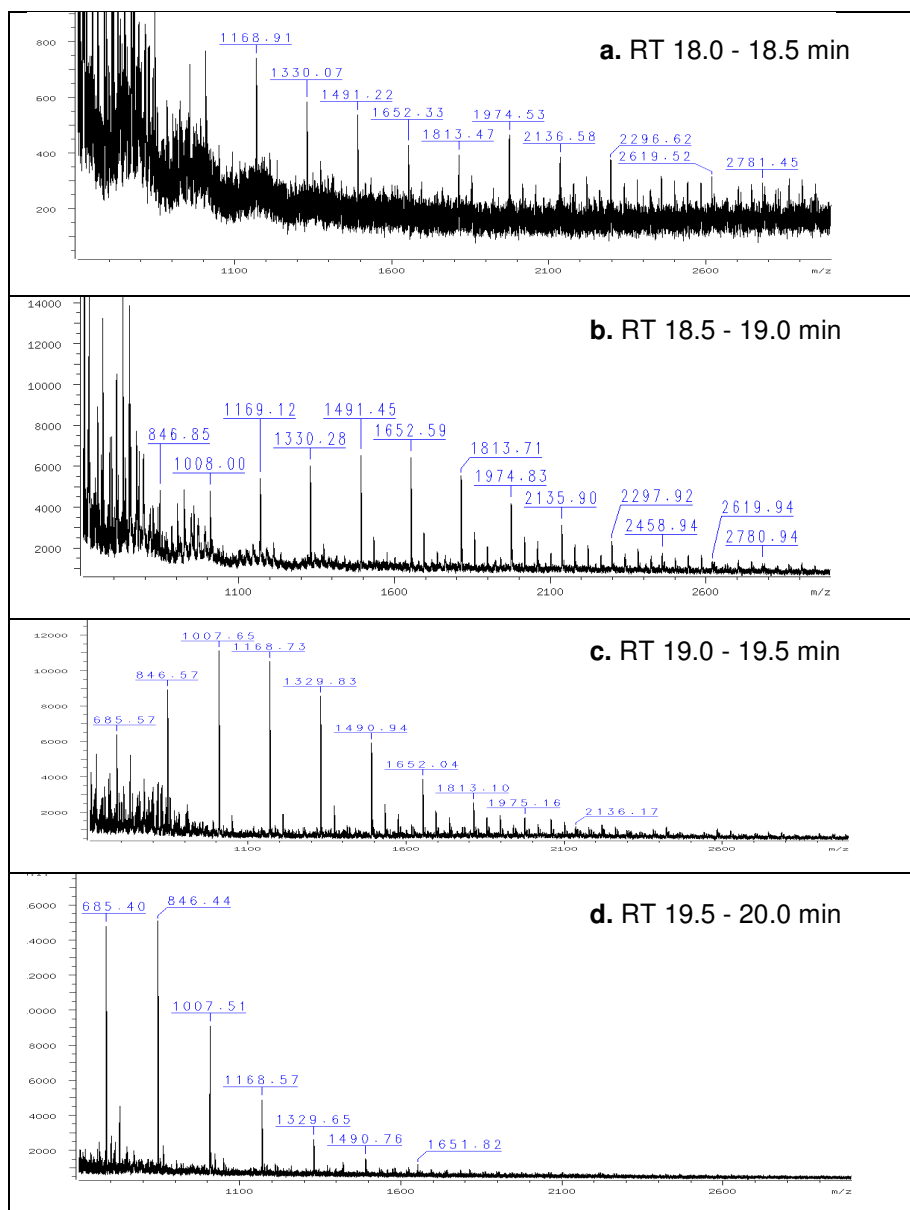


Figure 7. MALDI-TOF spectra (positive mode) of the collected GPC fractions at specified collection times.

It is already obvious right away that the MWs from GPC do not match that of the MALDI-MS. Another characterization tool was used, this time the ESI-MS. To do this, 1000 ug/mL solution of COS was prepared in deionized water. The COS solution was then introduced into the ESI-MS by direct infusion. into the APi 2000 MS-MS equipped with an electrospray chamber and triple quadrupole mass analyzer (Applied Biosystems). The analysis was carried out in q1 using the following ESI parameters: 5500 V ion spray voltage, 25 V cluster gas and 10 V ion source gas

1. The declustering potential (DCP) was set 100 V while the focusing and entrance potentials were at 400 V and 10 V respectively.

Figure 8 shows the positive mode ESI mass spectrum generated for the COS samples. ESI-MS instrument available in the laboratory has a quadrupole mass analyzer. Given this, the mass range is limited up to only 1800 Da. However because of the ability of the ESI to form multiply-charged ions, high molecular masses can still be analyzed in the MS. But even so, for chitosan, heavier chitosan were not detected in the MS.

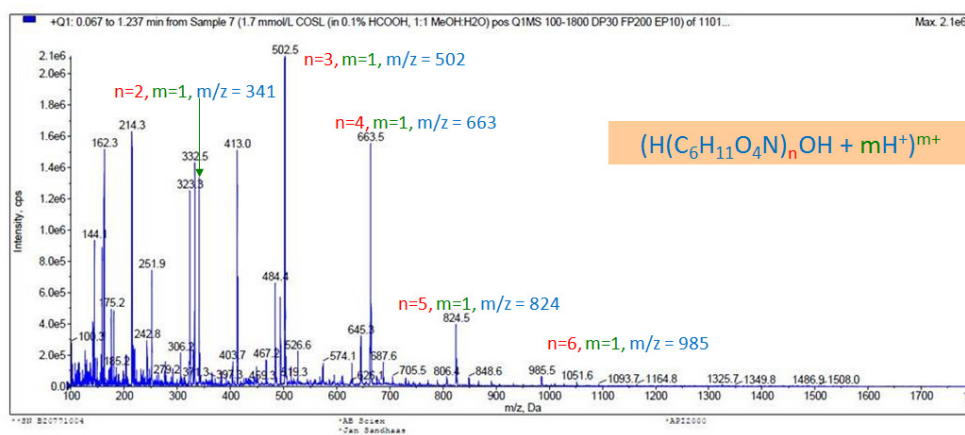


Figure 8. Positive mode ESI mass spectrum of COS.

This work shows that multi-technique approach is a better approach because it gives an overview of the methods being done and allows the analyst to think deeper into the limitations of the methods by comparison to other methods. In this work, it is revealed that GPC, MALDI-MS and ESI-MS give different estimate of the MW of chitosan oligosaccharide.

C. Interaction of Chitosan and Olive Oil

This section is an application of the first two sections under the main chapter on chitosan. The oil-binding property of chitosan was studied whether it can be a function of DD and DP. To determine DD, the IR-PLS method discussed in 2A was used while to determine DP, the GPC method in 2B was used.

The oil-binding capacity measures the ability of chitosan to interact with oil. To do this, chitosan is made to form a stable emulsion complex with olive oil. The excess olive oil (unbound oil) is separated from the stable complex and is measured gravimetrically.

The reported oil-binding capacity is expressed in percent. Based on its initial definition, oil-binding capacity does not consider the variable initial amount of chitosan used. To allow comparison, the results were normalized to 4.15 mg initial amount of chitosan and to 11.67 g olive oil used. The results of the oil-binding test are given in Table 4.

Table 4. Oil-binding capacity of the chitosan samples.

| Sample Code | Oil-binding capacity (%) | |
|-------------|--------------------------|-----|
| | Value | RSD |
| S1 | 40.1 | 2 |
| S2 | 86.5 | 7 |
| S3 | 33.4 | 1 |
| S4 | 38.3 | 10 |
| S5 | 52.1 | 8 |
| S6 | 22.7 | 16 |
| S7 | 77.8 | 18 |
| S8 | 35.7 | 8 |
| S9 | 44.2 | 12 |
| S10 | 27.1 | 10 |
| U1 | 62.8 | 2 |
| U2 | 69.0 | 1 |

The oil-binding capacity values represent the means and relative standard deviation (RSD) of 2 to 8 trial runs. It can be observed that some of the RSD of the data is up to almost 20%. The relatively low precision of the oil-binding test results from the low ruggedness of the method used. The neutral pH to which the chitosan-olive oil complex is to be stabilized was difficult to control.

To study the relationship of DP_w and DD versus oil-binding capacity, the values for chitosan S1 to S10 were put in a graph shown in Figure 3. Figure 9 represents in a 3D graph the general relationship between the variables DP_w and DD versus oil-binding capacity. A regression plane was drawn to visualize the general trend of the data. It can be observed that DD has a greater effect on the oil-binding capacity than DP_w as indicated by the steepness and direction of the slope of the regression plane. There is a clear negatively-sloped linear relationship between DD and oil-binding capacity despite the samples having a wide range of DP.

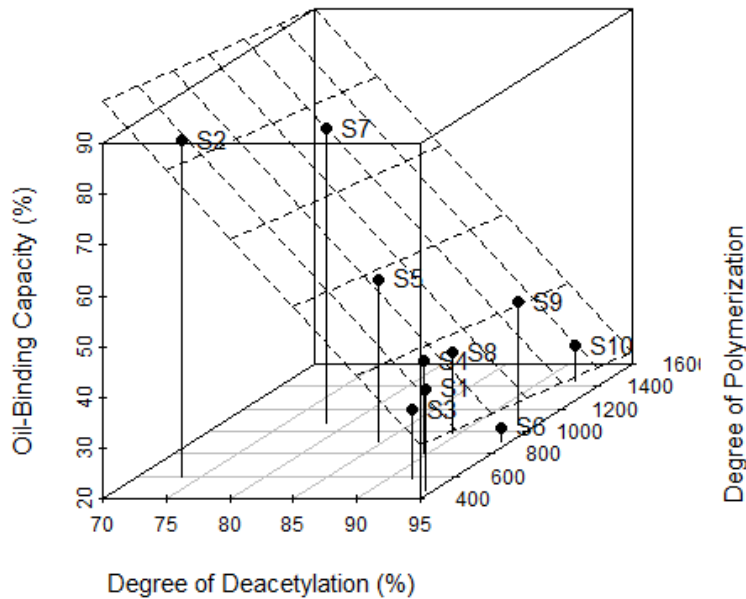


Figure 9. Relationship between Oil-Binding capacity to DD and DP.

PLS was used to correlate DD and DP_w to oil-binding capacity. Initially, PLS was generated using the S1 to S10 as the training set. The kernel algorithm used with the 'pls' function fitted the training set with only two variables (DD and DP_w), and the data was pre-treated by scaling prior to analysis [34]. Cross-validation of the generated model using the LOO had 9.6 % RMSEP if only one component was used and 9.1% if two components were used. The sources of the large prediction errors were the data coming from samples with low oil-binding capacities. The model with two components can only explain 89.2 % of the variations in oil-binding capacity.

The ability of the regression model to predict the oil-binding of chitosan given only the information on its DD and DP was tested using U1 and U2. Figure 10 shows the correlation between the experimental oil-binding capacity and the predicted oil-binding capacity for both the training set and the test set using the PLS model. The data points are scattered around the line experimental oil-binding capacity = predicted oil-binding capacity. The model's prediction of the training set is consistent with the result of the internal validation. The calculated % residuals for

the test sets were -4.5 % and -6.8 % for U1 and U2 respectively. The accuracy of the predicted value can only be as good as the precision of the experimental results used to derive the model.

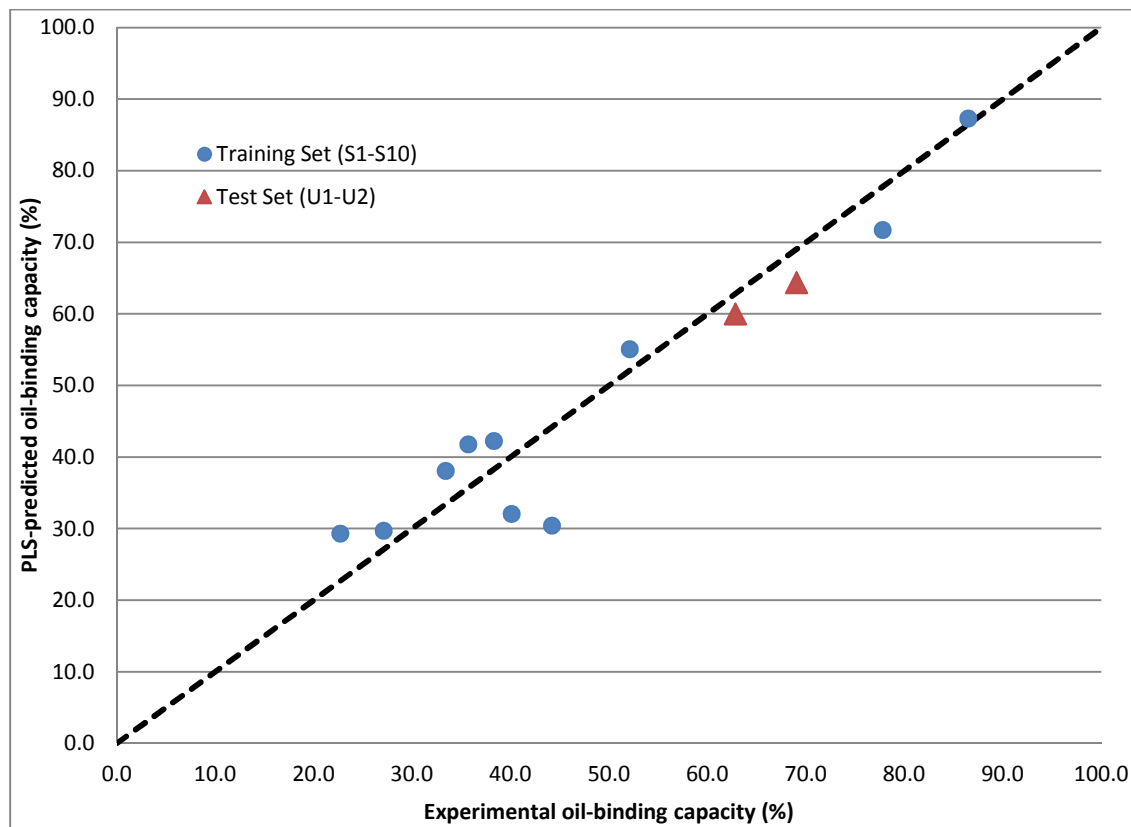


Figure 10. Comparison between the experimental oil-binding capacity and the PLS-predicted values-

The oil-binding capacity can be taken as a measure of the stability of emulsion of chitosan and olive oil in an aqueous environment at neutral pH. The olive oil used in the study is a mixture of at least 95% triacylglycerides (based on estimation) and the rest are diacylglycerides, monoacylglycerides and free fatty acids. The behavior of chitosan of a specific DD and DP under the conditions stated dictates its interaction with the glycerides and fatty acids. This can be explained by a number of mechanisms proposed in the literature [7].

It was shown that chitosan is capable of direct hydrophobic interaction with nonpolar molecules like cholesterol in the air-water interface and can directly eliminate them from aqueous solution. Simulation studies indicated that there are specific sites for interactions between chitosan and stearic acid or cholesterol. Results from a number of experiments shows that cholesterol in aqueous [24] and in nonpolar solvents such as chloroform [37] can interact with chitosan. The

increase in chain length (greater DP) increases the capacity of the chitosan for van der Waals interaction and thus the ability to bind with fat. However, for large polymers, conformation and folding in a complex aqueous system can decrease the interactions. It was shown in an *in vitro* study that at constant DD, high molecular weight chitosan adsorbed less cholesterol. In the same study, however, the effect of DD was unclear [24]. Zhou et al. also found the same trend for molecular size and the adsorption of olive oil by chitosan, however they have not found significant correlations between physico-chemical properties like DD and oil-binding capacity [29]. The hydrophobic interaction of chitosan with oil is not necessarily a one-to-one interaction. Chitosan was shown to act as an emulsifier providing mechanical and electrostatic stability to the oil droplets resulting to a stable water-oil-water multiple emulsions [38, 39].

A different mechanism suggests that chitosan, through the amino group of the glucosamine units, forms an insoluble salt by ionic interaction with bile acid anions [40]. These anions are characterized by an ionic end on one side a hydrophobic region on the other. The resulting insoluble salt is hydrophobic and can trap fats like cholesterol and triacylglycerides. A similar mechanism suggests the formation of micelle-like structure with bile salts that can trap fats in the inside. This is made possible with the amino and hydroxyl groups of chitosan acting as an interface between the bile acid anion and the aqueous environment respectively [41]. Like the bile acids, the free fatty acids in the oil can also interact with chitosan. A study on chitosan-lipid interactions in Langmuir monolayers suggests that fatty acids interact with chitosan in two steps: first is for the fatty acid to anchor in chitosan via electrostatic forces, then second hydrophobic interactions occur between the lipid tail of the fatty acid and chitosan forming the complex. The study noted that the bulkiness and saturation of the fatty acid can influence the interactions [42]. This resulting complex of free fatty acid and chitosan can further interact with oils.

At first look, there seems to be a contradiction between the two mechanisms discussed above in explaining the interaction of chitosan and olive oil. However, after considering that chitosan **behaves** differently in aqueous environment depending on its DD (Schatz et al., 2003), one can conclude that the two mechanisms in reality, complement each other. Chitosan in the domain $50\% < DD < 80\%$ behave in such a way that the hydrophobic and hydrophilic interaction in aqueous environment are counterbalanced. This domain is the interface between the highly electrostatic domain and the hydrophobic domain [17]. In this context, the first mechanism is favored. Chitosan without any need for additional surfactant can act as an emulsifier and interact directly with the triacylglycerides in olive oil. Based on the PLS model in the previous

section, DD has a negatively sloped linear correlation with oil-binding capacity suggesting that the chitosan – triacylglyceride interaction becomes stronger as the chitosan becomes acetylated and less polar. This model is consistent with the results of the study by Muzzarelli et al., where they percolated the olive oil in a column bed with chitin, chitosan or a chitosan derivative. The group found out that chitosan allowed more oil to be percolated through, while chitin on the contrary retained more of the olive oil. The authors also noted that the concentration of diacylglycerides (34 carbon and 36 carbon diacylglycerides) in the olive oil percolated in chitosan decreased compared with the original oil. On the other hand, the concentration of diacylglyceride was enriched in the percolated olive oil in chitin [43]. The trend of oil-binding capacity decreasing with DD can be extended up to DD of 90 % based on the PLS model. The PLS model points to hydrophobic interaction as the dominant intermolecular force of attraction that “binds” chitosan via the N-acetyl-D-glucosamine monomers and olive oil triacylglycerides (Figure 11A).

At the region of very high DD (DD > 90 %) the negatively sloped linear correlation tends to be diminished. The amount of N-acetyl-D-glucosamine monomers limits the direct hydrophobic interaction of chitosan to olive oil triacylglycerides. It is inferred that on this region, the 2nd mechanism is favored. The free oleic acid interacts electrostatically with the amine group of the D-glucosamine monomers while at the same time also interacts via hydrophobic forces with olive oil (Figure 11B). Under this mechanism, it is expected that as DD is increased, oil-binding capacity should increase.

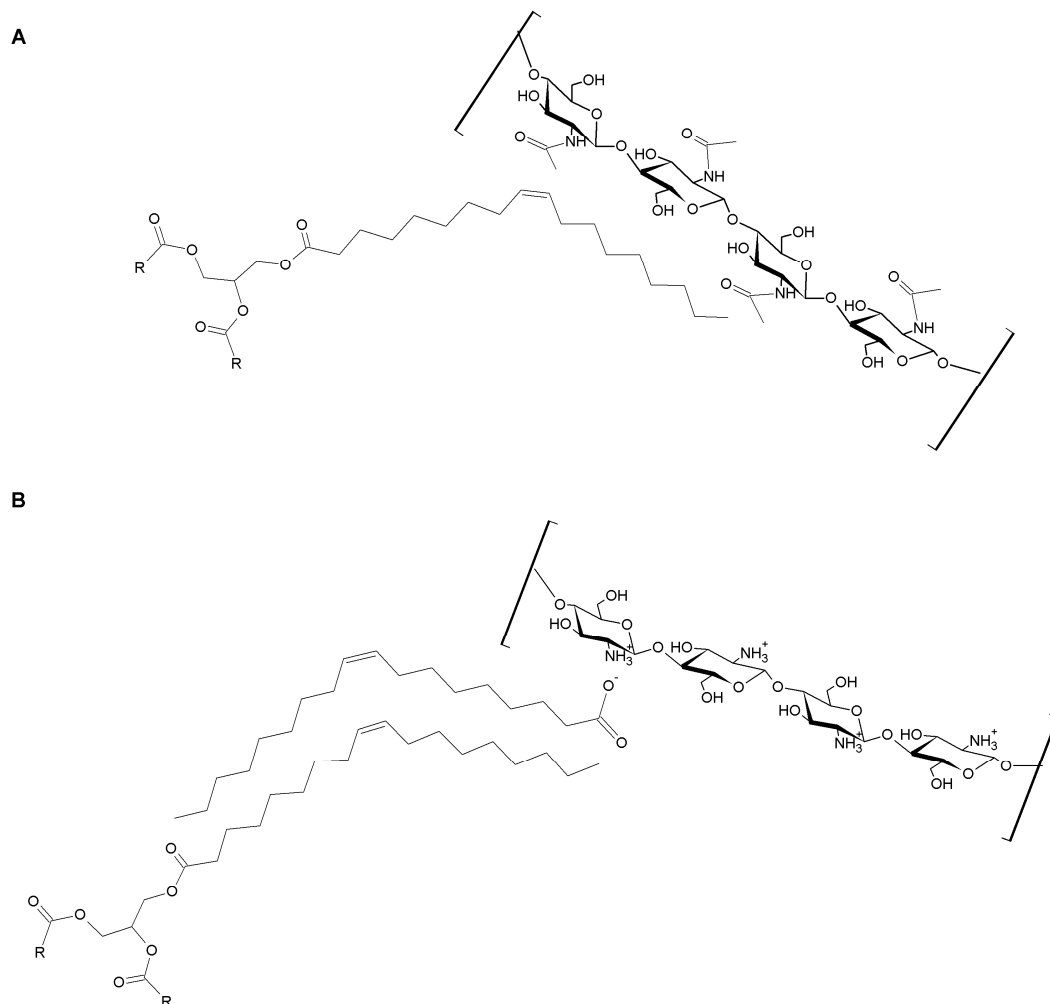


Figure 10. Mechanism of interactions of chitosan with olive oil: A. Direct hydrophobic interactions and B. Interaction with the aid of free fatty acids.

III. Oligosiloxanes

The oligosiloxane was synthesized in-house. The process involved the acid-catalyzed polymerization of 3-triethoxysilylpropan-1-amine. Figure 12 shows the proposed general scheme of the reaction. The three ethoxy groups are first hydrolyzed forming 3-trihydroxysilylpropan-1-amine. Then, at least two molecules of 3-trihydroxysilylpropan-1-amine condense to form the siloxane chain. In Figure 1, for the purpose of simplification, only the dimer product is shown. The polymerization process, however, can produce a variety of products that differ primarily in the number of monomer units or degree of polymerization (n). Variety can also result from molecules of the same degree of polymerization but differ in the

extent of water elimination during the intramolecular reactions of the remaining hydroxyl groups. The possibility of forming cyclic products adds to the diversity in the molecular weight distribution of the oligosiloxane.

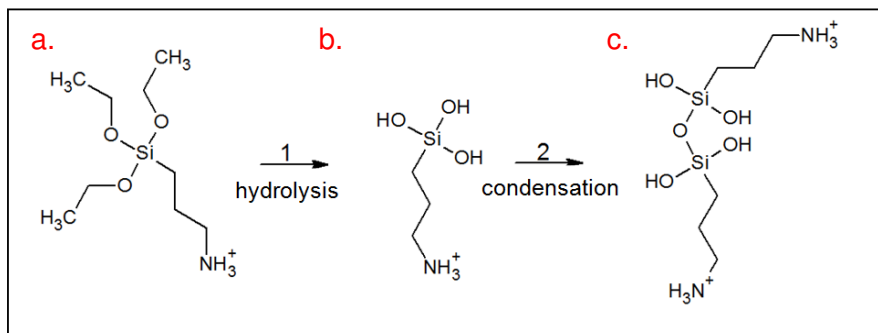


Figure 12. Proposed general scheme in the acid-catalyzed formation of the oligosiloxane: a. 3-triethoxysilylpropan-1-amine; b. 3-trihydroxysilylpropan-1-amine; c. dimer

The average molecular weights and the polydispersity data derived from classical techniques such as gel permeation chromatography (GPC) can be a way of characterizing the oligomers such as the oligosiloxane. However, this technique can give a relative result depending on the molecular weight standards used. Knowledge of the absolute molecular weights and hints on the possible structure of molecules present in the oligomer distribution can be useful in multiple ways including in studies on structure-properties-use and on compliance to European environmental guidelines like the Registration, Evaluation, Authorization and Restriction of Chemical Substances (REACH).

In this project, the molecular weight of the individual homologues and the oligomer distribution of the oligosiloxane synthesized in-house from 3-triethoxysilylpropan-1-amine were studied using ESI- and MALDI-MS in combination with analytical techniques such as liquid chromatography (LC) and induced coupled plasma – atomic emission spectrophotometry (ICP-AES).

A novel method was developed to determine the molecular weight distribution of oligosiloxane. The method involved separation of the homologues of the oligosiloxane in a C18 column with perfluoroheptanoic acid as an ion pair reagent in the gradient of water and methanol as eluent. Electrospray-q1 mass spectrometry (ESI-q1 MS) showed that the oligosiloxane had a degree of polymerization of 3 to 14. Single homologue standards were then prepared by collecting

fractions at specific retention times. The homologue concentration in each solution was determined using induced-coupled plasma optical emission spectrophotometry (ICP-OES) at 212 nm emission of Si atom. Quantification of the homologues of oligosiloxane was done using ion pair chromatography interfaced to ESI-q1 MS in the multiple ion monitoring mode and with the single homologue solutions as calibration standards.

A. MS of the oligosiloxane prior to fractionation

ESI-q MS and MALDI-ToF MS were used in complement with each other to get a glimpse of the molecular weights of the individual molecules present in the oligosiloxane formulation. Figures 13a and 13b show the positive-mode mass spectrum generated from the ESI-q MS and MALDI-ToF MS, respectively.

The ESI-q mass spectrum shows that the oligosiloxane homologues present have a degree of polymerization in the range from 1 to 12. It can be observed that the expected molecular weights of ions resulting from condensation of the monomer were not present, assuming that NOT only polymerization had occurred. For example, for $n=6$, the expected m/z value of the ion that would appear in the mass spectrum is 733 Da accounting for the six molecules of trihydroxy-3-aminopropylsilane monomer minus five water molecules lost during condensation and an addition of a proton for the ionized form. Nowhere can one find 733 Da in the ESI-q mass spectrum, but instead one finds significantly lower masses. The insert in Figure 2a shows the ion masses (assuming a charge of +1) that can be attributed to $n=6$. It shows a pattern with 18 Da difference (in the figure, the Δ 17 Da results from rounding error). The ions at m/z 661, 643, 625 and 608 are substantially smaller than the expected ion mass. Calculations reveal that these are the resulting masses after the parent mass lost 4, 5, 6 and 7 more water molecules, respectively. It is difficult to assess at which step the further elimination of water occurred.

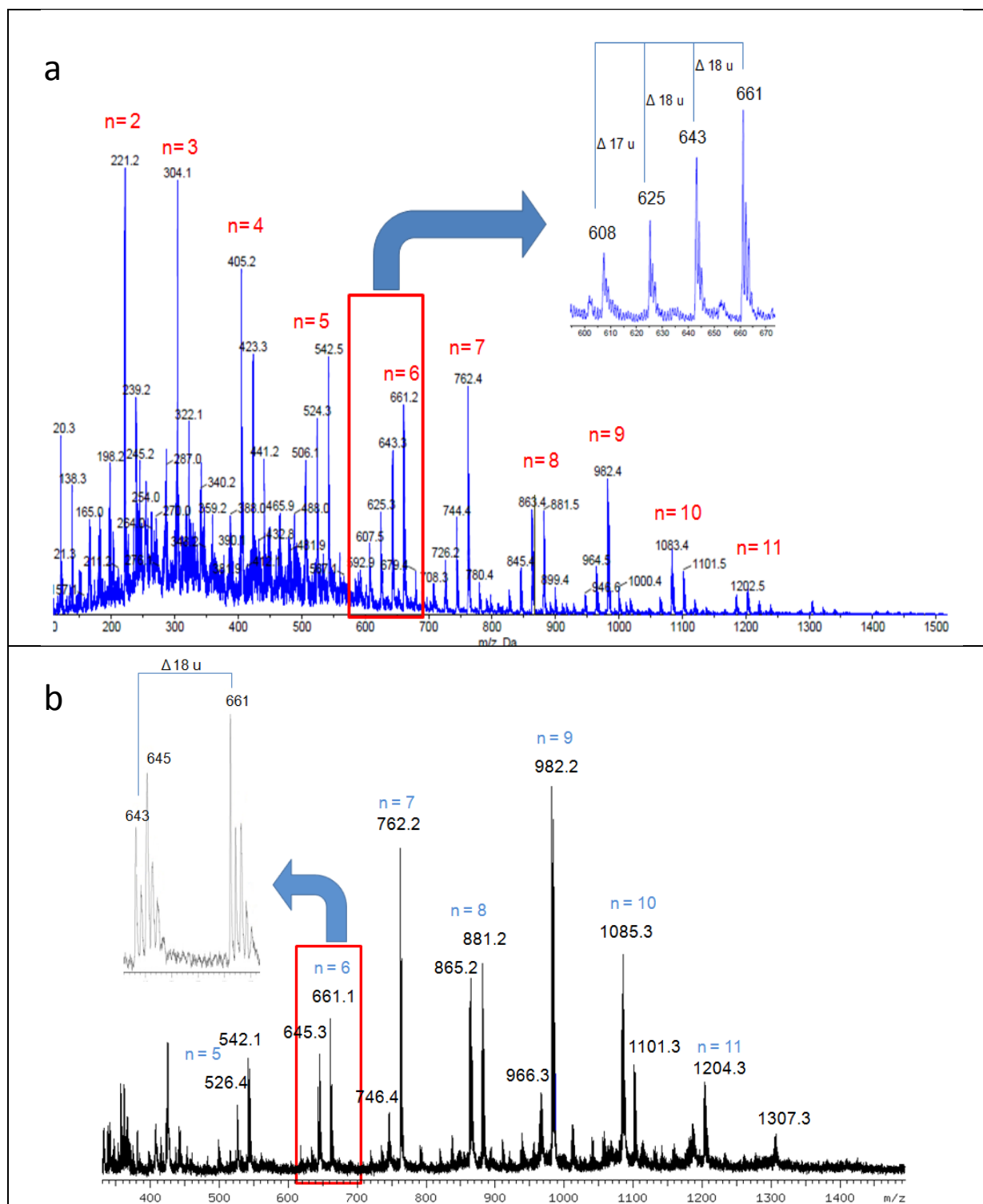


Figure 13. Positive-mode mass spectra of oligosiloxane: a. ESI-q at declustering potential of 160 V, formulation was diluted 1+9 in methanol; b. MALDI-ToF, with 2,5-dihydroxybenzoic acid as matrix; n represents the degree of polymerization

MALDI-ToF MS was done as a complementary method in determining the molecular weights of the oligosiloxanes. The generated MALDI-ToF mass spectrum was notably different compared to the one generated by ESI-q. First, the lower molecular weight oligosiloxanes ($n < 5$) were not readily observed in the MALDI mass spectrum since the region below 500 Da is always filled with signals from matrix ion clusters. The matrix used in this analysis was 2,5-dihydroxybenzoic acid. This matrix always generates a variety of cluster ions that saturates the region below 500 Da. Secondly, not much water loss was observed in MALDI. For example, again for $n=6$, only ion m/z 661 and 643 (see Figure 13b insert) were observed in significant amount. In the matrix-assisted ionization of oligosiloxane, unlike in ESI, there is no declustering needed because the molecules are ionized from the dried samples using very short laser pulses. As a consequence, in MALDI, less decomposition is expected. From this observation, one can infer that the ion masses 661 and 643 Da could be associated with the forms of the oligosiloxanes in the formulation whereas ion masses 625 and 608 (which are only found in the ESI-q mass spectrum) are resulting from fragmentation during the ESI process. Lastly, the relative intensities of the ion masses are not the same in ESI-q and in MALDI-ToF mass spectra. This difference is expected and is not unique to oligosiloxanes. Neither the ESI-q nor the MALDI-ToF mass spectrum represents the real distribution of the oligosiloxanes. It is a well-known problem in the mass spectrometry of oligomers/polymers that there is a sensitivity bias against the higher molecular weight components. This bias is due to the difficulty in ionizing large molecules and in detecting them. In ESI-q MS, the formation of multiply-charged ions contributes to the complexity in estimating the relative counts of each structurally unique ions. This will be discussed in more details in the next section.

The ESI-q and MALDI-ToF direct mass spectrometric analysis of the oligosiloxane formulation gave a general overview or hint on the kind of oligosiloxane species present in the formulation. While there are hints, the combined ESI-q and MALDI-ToF MS was not really able to absolutely tell the extent of water elimination in the formulation and differentiate this from water elimination in the MS. The methods, also, are unable to give accurate information on the relative abundance of the species present in the formulation. To gain insight on the oligomer distribution, it would be necessary to separate the individual species in the fraction and to quantify those using standard reagents. The next sections describe the development of method to achieve these goals.

B. Fractionation of the oligosiloxane

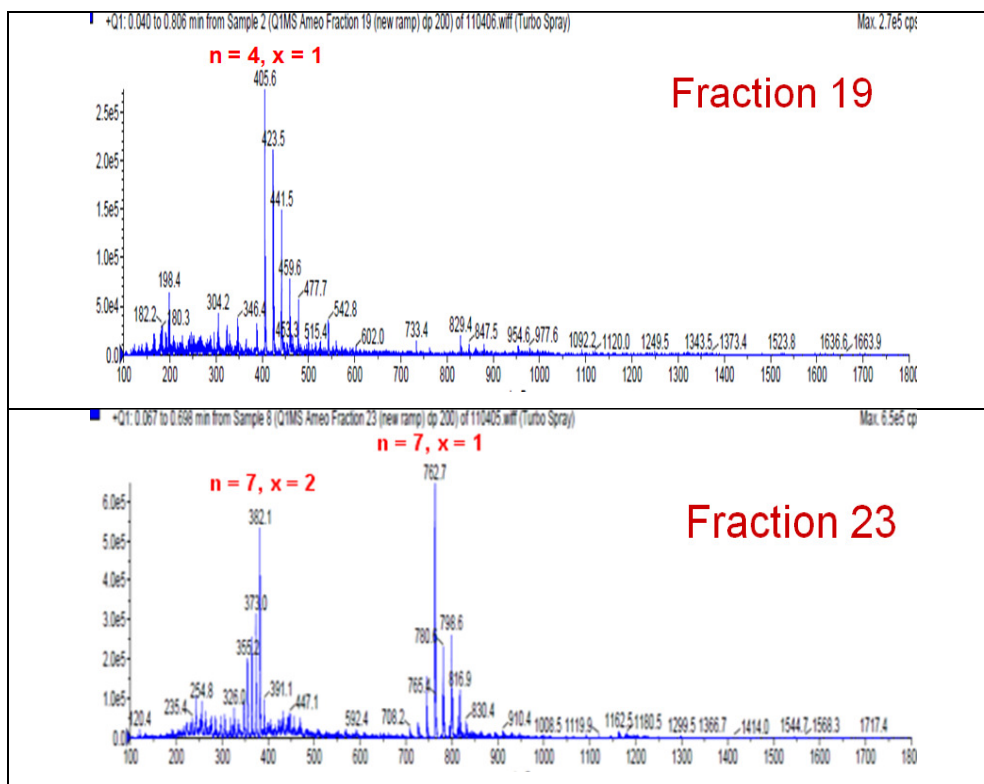
Table 5. Detected oligosiloxane in each of the collected fraction in the region between 37.0 min. and 42.6 min.

| Fraction* | Retention Time (min) | Detected Oligosiloxane Homologue (n) |
|-----------|----------------------|--------------------------------------|
| 17 | 37.0 – 37.4 | 3 |
| 18 | 37.4 – 37.8 | 3, 4 |
| 19 | 37.8 – 38.2 | 4 |
| 20 | 38.2 – 38.6 | 5 |
| 21 | 38.6 – 39.0 | 6 |
| 22 | 39.0 – 39.4 | 6 |
| 23 | 39.4 – 39.8 | 7 |
| 24 | 39.8 – 40.2 | 8 |
| 25 | 40.2 – 40.6 | 8, 9 |
| 26 | 40.6 – 41.0 | 10 |
| 27 | 41.0 – 41.4 | 10 |
| 28 | 41.4 – 41.8 | 11 |
| 29 | 41.8 – 42.2 | 11, 12 |
| 30 | 42.2 – 42.6 | 12 |

*The number labels of the fractions are arbitrary and could differ from one run to another. Nonetheless, the fraction number is included in the table for easy references to the ESI-q mass spectra in Appendix. The more important parameter is the retention time interval (2nd column) in which a certain fraction is collected.

Table 5 summarizes the homologues detected at each collected fraction in the region. It can be observed that not all homologues were entirely separated during fractionation. This is not a problem since there are also fractions that contain single homologues (e.g. fractions 17; 21 and 22; and 26 and 27 that contains homologues of n= 3; 6; and 10 respectively). More of these single-homologue containing fractions will be collected and will be developed as oligosiloxane standards.

The mass spectra of fractions 19, 23 and 28 containing homologues with $n = 4, 7$ and 11 respectively are shown in Figure 15. It can be observed that at higher n , multiply-charged ions are favored by the ESI process. For example, at $n=7$ (fraction 23), two patterns of the same compound appear in the mass spectrum. One form results from the singly charged compound while the other form originates from doubly-charged compound. The mass differences of 18 and 9 for these forms reflect the loss of water from singly- and doubly- charged molecules, respectively. For $n=11$ (Fraction 28), the singly-charged form occurred minimally while the doubly- and triply-charged forms are more pronounced. Multiple-charging is highly reasonable at higher n since the number of amine groups that can accept extra protons is proportional to n . This is an important observation that must be taken into consideration in the future if one is to use ESI-q MS in the quantification of the individual homologue and in establishing an accurate distribution for the oligosiloxane.



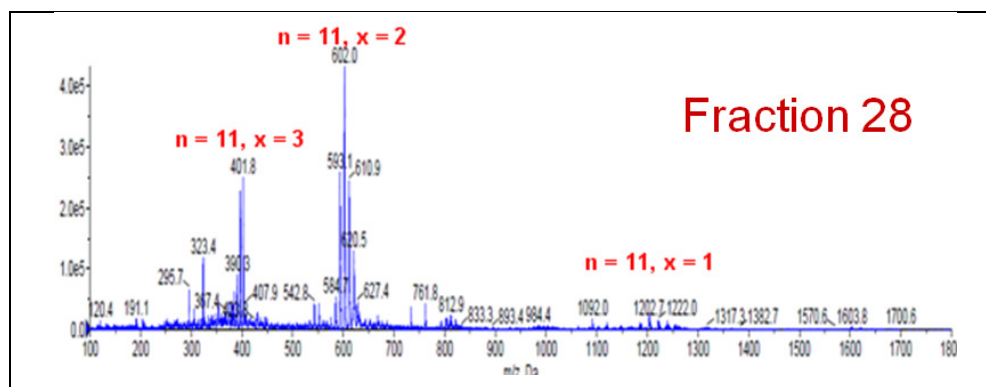


Figure 15. Positive-mode ESI-q mass spectra of Fractions 19, 23 and 28 containing oligosiloxanes of $n= 4, 7$ and 11 respectively. x represents the charge of the ions.

C. ICP-OES

Induced coupled plasma – optical emission spectroscopy (ICP-OES) method was further validated for the determination of the absolute amount of oligosiloxane homologue in a solution. The behavior of the Si optical lines in the presence of matrix substances was investigated. Figure 16 shows the optical emission spectra related to Si for the oligosaccharide in water with perfluoroheptanoic acid as a matrix. It can be observed that the spectral line at 152.67 nm is affected by the addition of PFHA. The other Si spectral emission lines are less affected by PFHA. Figure 17 shows the calibration curve generated for the standards. The matrix effect is observed in the calibration curve using the emission at 152.67 nm with the shift in the slope of the linear function.

Aside from having the less change in the slope of the calibration curve, the emission at spectral line at 212.41 nm had the most reproducible signal and gave a detection limit down to 0.1 ug/mL. Figure 2 shows the emission spectra at 212.4 of a blank, and standard solutions of siloxane at 0.1 and 0.5 ug/mL concentration. The instrumental limit of detection therefore can safely be set at 0.1 ug/mL.

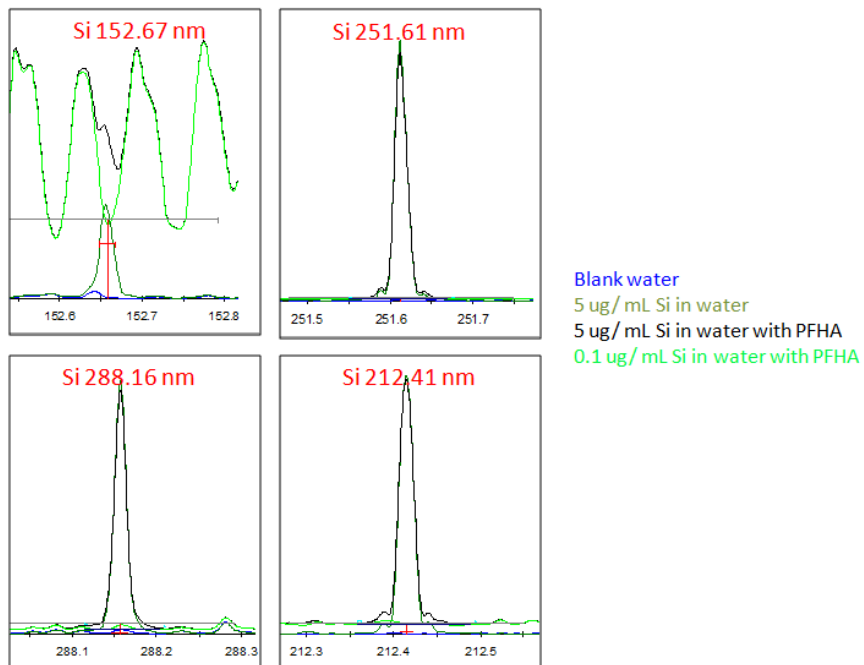


Figure 16. Si optical emission lines of oligosiloxane.

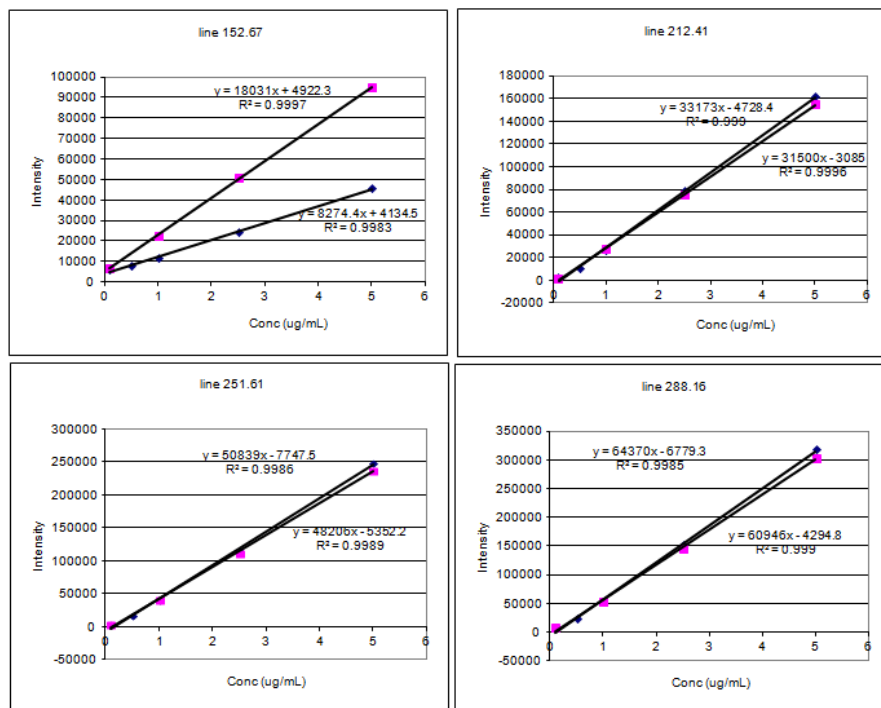


Figure 17. Calibration curve of oligosiloxane in water (pink square) and in water with PFHA (blue diamond).

In summary for oligosiloxanes, multi-technique approach enables the separation and quantification of the homologues that are not separated well by GPC.

III. Polyethylene glycol (PEG) and PEG-based nonionic surfactants

Liquid chromatography (LC) is used in tandem with MS for polymer characterization in two ways: 1.) to separate highly polydispersed polymers by their molecular weights using size-exclusion; and/or 2.) to separate polymer mixtures by their overall polarity through partitioning. Online coupling of LC with ESI and/or MALDI are possible.

Polymers can be mixture of molecules with the same backbone structure but different end groups. Direct MS analysis of polymer mixtures can be a difficult task. First, there could be ionization bias depending on the nature of the end group. Secondly, the mass spectrum of a polymer mixture is complex and difficult to interpret. Partition chromatography can be employed to separate the polymer components firsts based on the polarity of the end group prior to analysis by MS.

In their study, Lee et al. used partition chromatography to separate the trace polymer impurities in fatty alcohol ethoxylates prior to MS. These impurities are the unreacted PEG and the ethoxylates with the undesired end group. The undesirable end group varies from the desirable ones only with the length of the fatty acid chain. The trace impurities cannot be determined directly by MALDI-TOF MS because the signal of the major components will shelve that of the trace impurities. Separation of impurities and the major components was done in an octadecyl (C18) column based on the polarity of the end group [44].

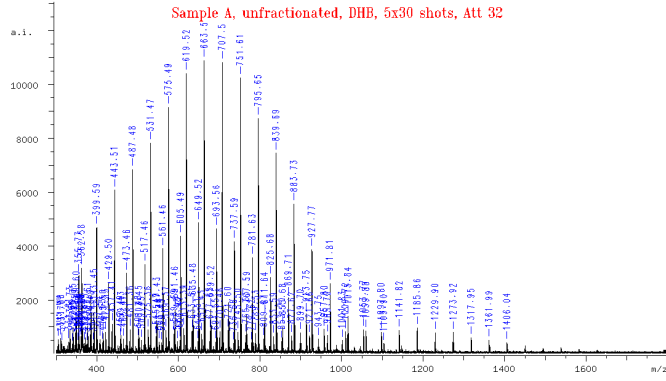
In this project, the composition of two detergent types supposedly differing in the composition of ethoxylated nonionic surfactants was elucidated using matrix-assisted laser desorption ionization - time of flight mass spectrometry (MALDI-TOF MS). The generated mass spectrum

of each surfactant mix in 2,5-dihydroxybenzoic acid (DHB) matrix showed two or more different ethoxylate distributions.

To further characterize the mixes, fractionation by reverse-phase high performance liquid chromatography (RP-HPLC) was done. The retention time gave additional information on the polarity of the polymer components. For comparison, standard polyethylene glycol (PEG) was also analyzed.

The two surfactant mixes (Samples A and B) and a polyethylene glycol standard (Sample C, control) were dissolved in sufficient amount of deionized water and were analyzed in the MALDI-TOF MS with DHB as matrix. Figure 18 (a-c) shows the generated mass spectra of the samples in the positive ionization mode without chromatographic separation.

a. Sample A



The mass distribution of the PEG standard (Fig. 1 c) can be assigned as follows:

$\text{HO}-(\text{CH}_2-\text{CH}_2-\text{O})_n-\text{H} + \text{Na}^+$ or $+ \text{K}^+$; e.g. for

$n = 20 + 23 (\text{Na}^+) m/z = \mathbf{921 \text{ u}}$ and for $n = 20 + 39 (\text{K}^+) m/z = \mathbf{937 \text{ u}}$.

The MS-spectrum of Sample "A" (Fig. 1 a) shows a bimodal distribution resulting from PEG and Genapol X-080. The mass distribution of the Genapol X-080 can be assigned as follows:

$\text{CH}_3-(\text{CH}_2)_{12}-\text{O}-(\text{CH}_2-\text{CH}_2-\text{O})_n-\text{H} + \text{Na}^+$ or $+ \text{K}^+$; e.g. for

$n = 13 + 23 (\text{Na}^+) m/z = \mathbf{795 \text{ u}}$ and for $n = 130 + 39 (\text{K}^+) m/z = \mathbf{811 \text{ u}}$.

The MS-spectrum of Sample "B" (Fig. 1 b) shows mainly a distribution resulting from Genapol X-080.

Unlike that of the PEG standard, the mass spectra of the surfactant mixes are composed of at least two distributions indicating that the mixes have at least two components. In any of those distributions, the difference between masses is always 44, suggesting that the main polymer backbone of the components is ethoxylate and they are most likely differing only in their end groups.

Based on visual inspection of the mass spectra, surfactant A has at least 3 components while surfactant B has only at least two components. Genapol X-080 is the major component of both Sample A and Sample B.

To further characterize the mixes, fractionation by reverse-phase high performance liquid chromatography (RP-HPLC) was done. The separation of the different components in the mixes was achieved in a C18 column with pure methanol as the mobile phase. To detect the ethoxylates, the absorbances of the solution at 220 and 240 nm were monitored using a diode array detector (DAD).

Figure 19 (a-c) shows the generated chromatograms of the two surfactant mixes and the PEG standard by monitoring the absorbance at 220 nm of the DAD. By visual inspection, it can be

observed that sample A has at least 5 components; sample B has at least 3; and the control has only one component.

Fractions of the samples at each chromatographic peak were collected and were analyzed in the MALDI-TOF MS. The boxes in the figures were added to denote the retention time when the fractions were collected. The blue boxes represent the fraction with no ethoxylate detected in the MALDI-TOF MS. Meanwhile, the red boxes represent the fractions that contain the ethoxylates. The roman numerals give the link to the corresponding mass spectrum in Figure 20.

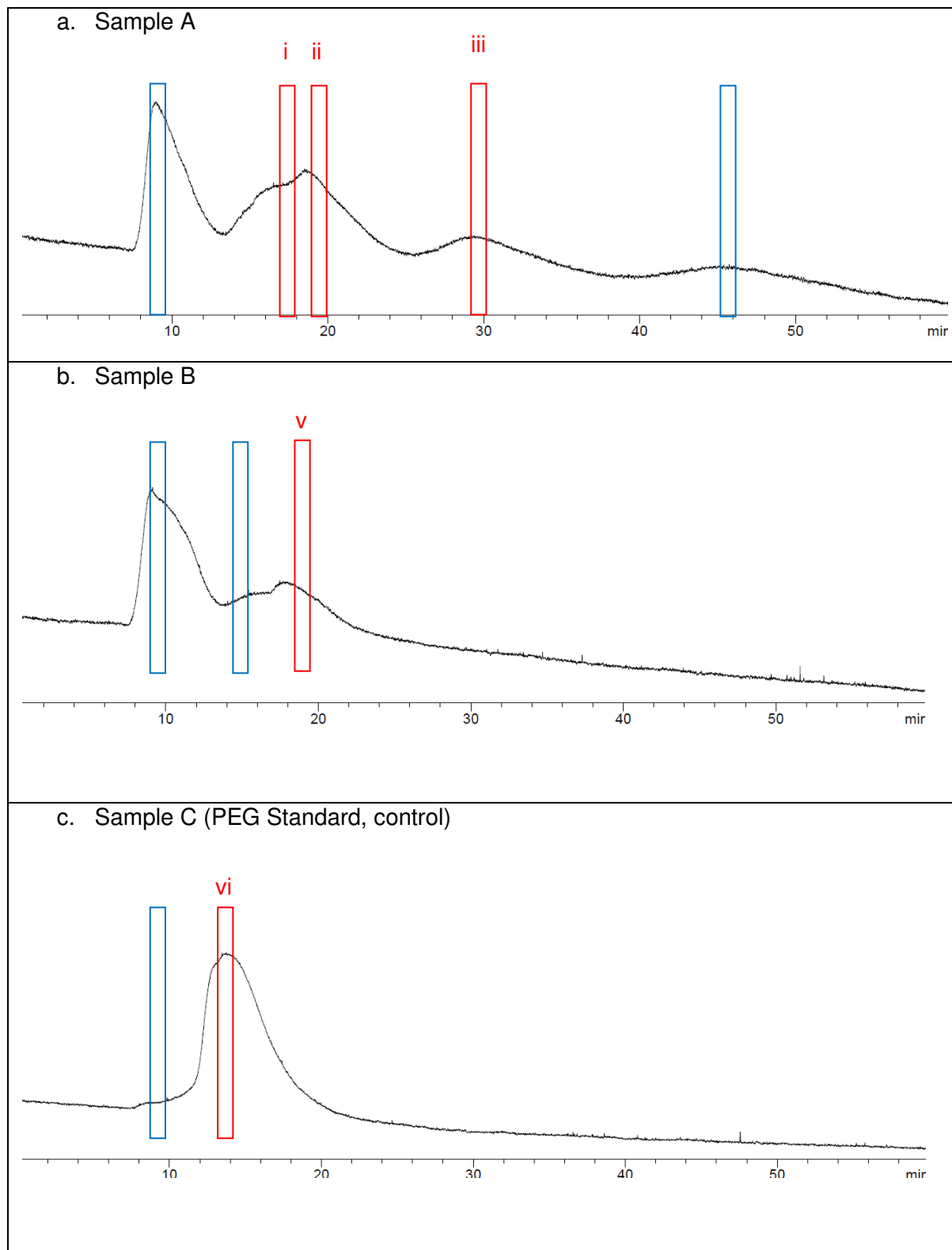
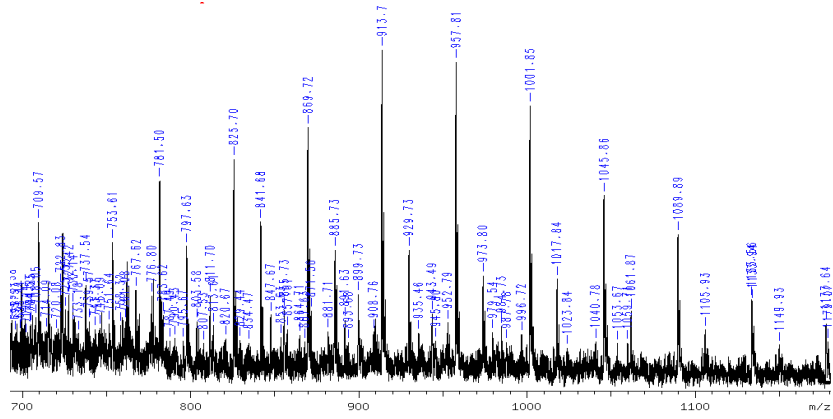
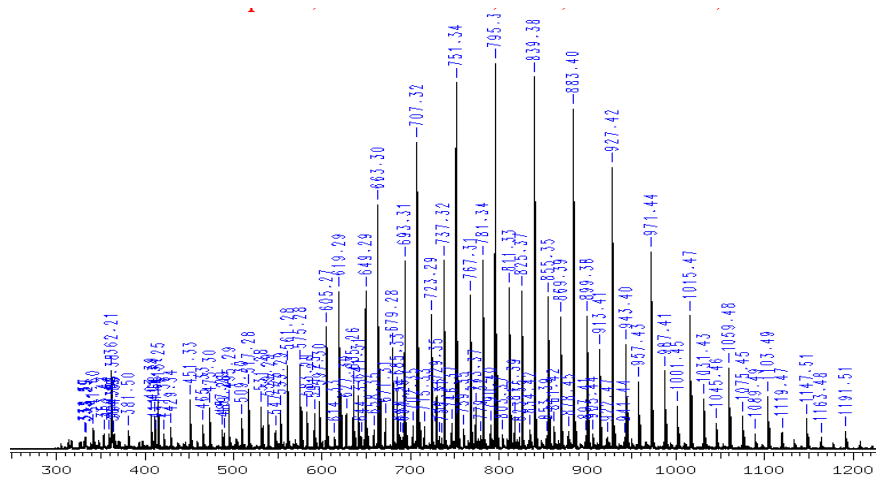


Figure 19. RP-HPLC analysis of the surfactant mix samples (a and b) and PEG standard (c).

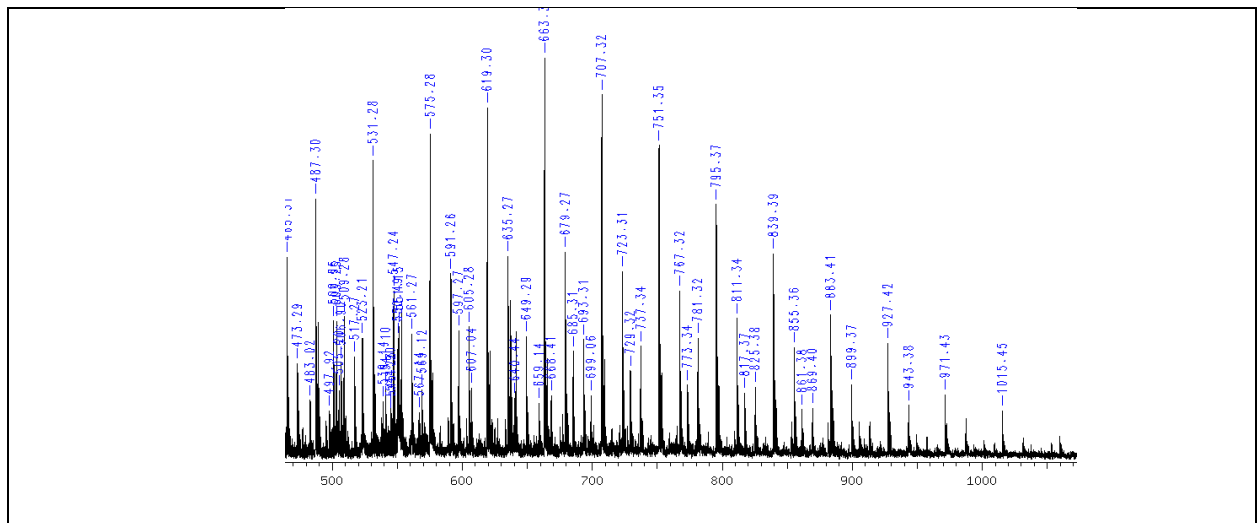
i. Sample A at RT 17.0 minutes



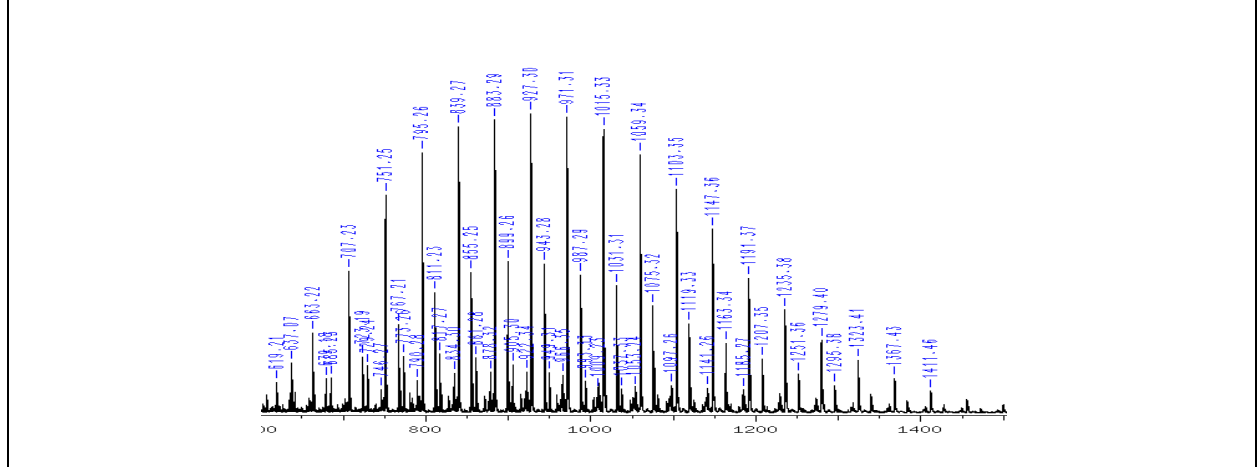
ii. Sample A at RT 19.0 minutes



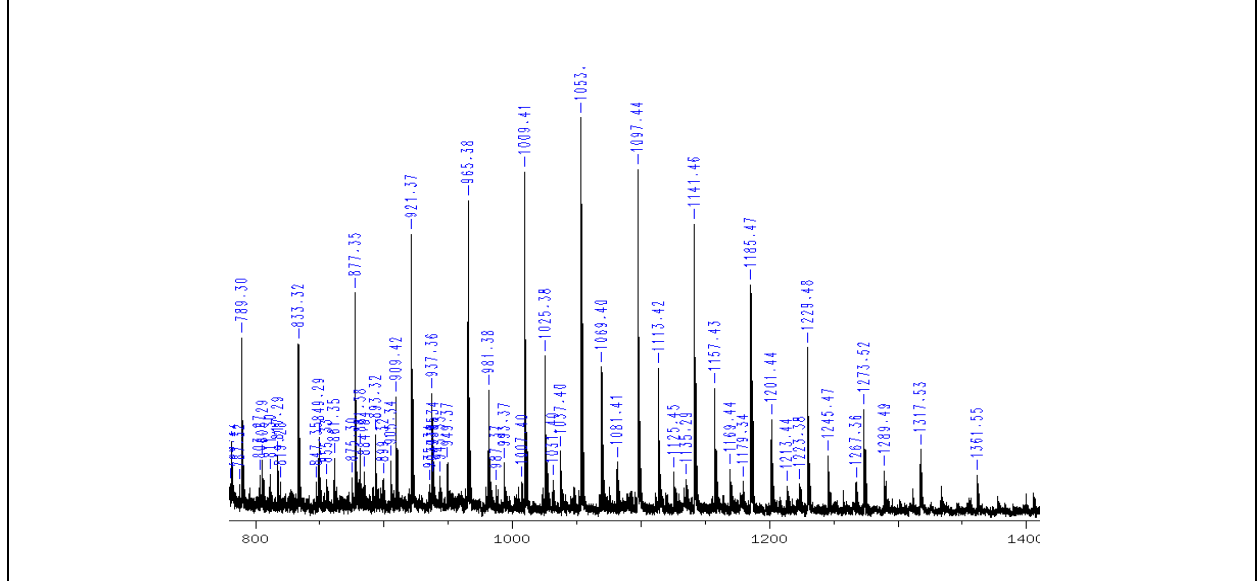
iii. Sample A at RT 30.0 minutes



iv. Sample B at RT 19.0 minutes



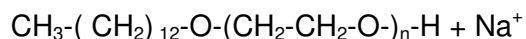
v. Sample C (control) at RT 14.0 minutes



Only one fraction of the **PEG standard** gave a spectrum with polymer distribution. The spectrum generated by the fraction at 14.0 mins. of PEG standard (Fig. 20v) is similar to the spectrum of the unfractionated PEG standard (Fig. 18a).

For sample A, HPLC was able to separate the components in the mixture into three distinct peaks. The first to elute at retention time (RT) 17 mins. (i) has a distribution similar to the PEG standard, ethoxylates with hydroxyl end group. The second peak (at RT 19 mins.) is a mixture of ethoxylates that include the Genapol X-080 (ii). The third peak (at RT 30 mins.) is gives a similar MALDI-TOF spectrum as that of the second peak (iii).

Figure 21 shows the zoomed in region (m/z 700 – 800 u) of the MALDI-TOF spectrum of the Sample A fraction collected at RT 19 mins (ii). The main signals m/z 707, 751 and 795 u can be assigned as Na^+ adducts of Genapol X-080:



$$n = 11-13$$

The m/z 723 and 767 u can be assigned as the K^+ adducts of Genapol X-080. These signals can also be assigned as follows:



where $x + y = 10$ and $n = 12$ and 13 respectively.

Likewise, m/z 737 and 781 u can be assigned as follows:



where $x + y = 11$ and $n = 12$ and 13 respectively.

and m/z 729 and 773 u can be assigned as follows:



where $x + y = 2$ and $n = 15$ and 16 respectively.

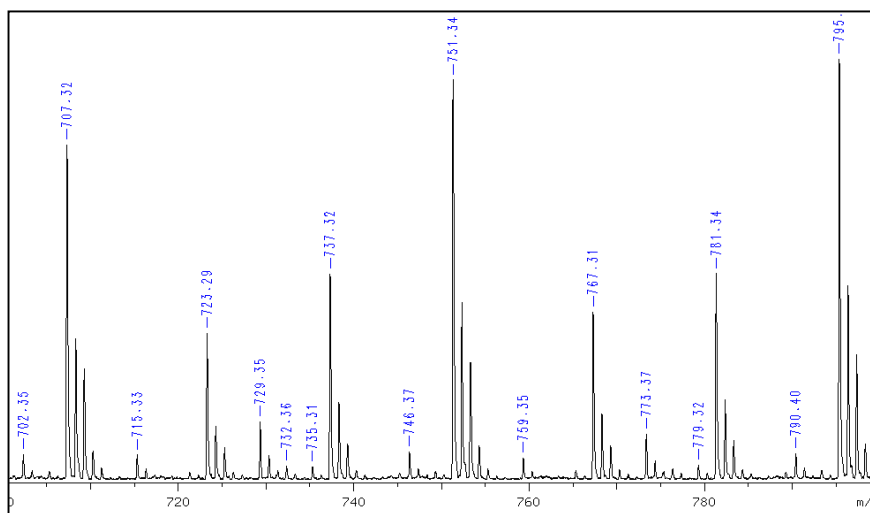


Figure 21. Region m/z 700 – 800 u of the MALDI-TOF spectrum of the Sample A fraction collected at RT 19 mins.

The fact that all the three ethoxylates eluted at the same retention time indicates that these components have similar polarities even if there is a difference of 1 or 2 carbons in the alkyl chain.

Interestingly, for sample A, the fraction collected at RT 30 mins. (Fig. 20iii) gives a similar MALDI-TOF spectrum as that of the fraction collected at RT 19 mins (Fig. 20ii). It can be inferred that the components could be constitutional isomers of each other but with a difference in their polarities making them elute at different retention times in a C18 columns.

For sample B, HPLC was not able to separate the ethoxylates suggesting that the components have similar polarity. Moreover, the MALDI-TOF spectrum of the fraction at RT 19 mins. (Fig. 20iv) is comparable to that of the unfractionated sample (Fig 18b).

Figure 22 shows the zoomed in region (m/z 700 – 800 u) of the MALDI-TOF spectrum of the Sample B fraction collected at RT 19 mins (ii). The signals at m/z 707, 723, 729, 751, 767, 773 and 795 u can be assigned in the same way as in sample A (Figure 21). In contrast to that of sample A, sample B does not have m/z 737 and 781 u.

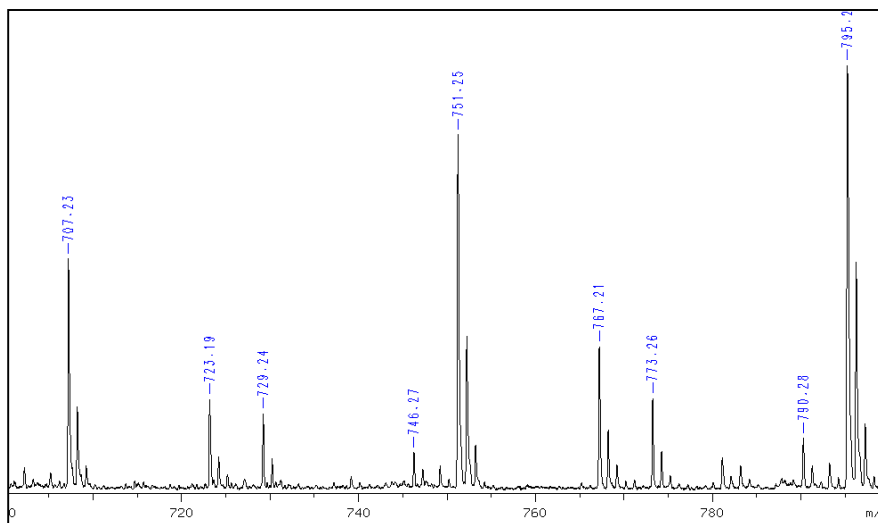
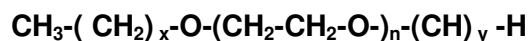


Figure 22. Region m/z 700 – 800 u of the MALDI-TOF spectrum of the Sample B fraction collected at RT 19 mins.

The observed difference in the cloud point of both surfactants corresponds to structural differences in the surfactant mixtures. In summary, the components of both surfactant samples A and B can be in the general form:



where $x + y$ is responsible for the varying distributions observed. Table 6 below summarizes our findings.

Table 6. Summary of the observed pattern for ethoxylates where x and y corresponds to the subscripts in the molecular formula: $\text{CH}_3-(\text{CH}_2)_x-\text{O}-(\text{CH}_2-\text{CH}_2-\text{O})_n-(\text{CH}_2)_y-\text{H}$

| Distribution | Sample A | Sample B |
|--------------------------------|----------|--------------|
| x=12 (Genapol X-080) | detected | detected |
| x=0, y=0 (hydroxyl end groups) | detected | not detected |
| x+y = 10 | detected | detected |
| x+y = 11 | detected | not detected |
| x+y = 2 | detected | detected |

V. Summary

Polymers are large molecules composed of repeating units called monomers. Polymers vary in terms of the monomer/s used; the number, distribution and type of linkage of monomers per molecule; and the side chains and end groups attached. Given this diversity, traditional single-technique approaches to characterization are often limited and inadequate, especially to polar synthetic polymers. Under this ECO-ITN fellowship, multi-technique but polymer-specific approach was found to be an appropriate alternative. This strategy was applied in characterizing chitosan and COS, oligosiloxanes and ethoxylates.

Infrared (IR) spectroscopy with partial least squares (PLS) chemometric technique was used to determine the degree of deacetylation (DD) of chitosan samples. The values obtained for chitosan samples with unknown DD using IR-PLS were comparable to the values obtained by potentiometric titration. IR-PLS has the advantage of being more precise and rugged than the other methods.

Size exclusion chromatography (SEC) coupled offline to matrix-assisted laser desorption ionization mass spectrometry (MALDI-MS) was used to determine the average molecular weights (MW) of chitosan oligosaccharide (COS). The average molecular weights obtained by MALDI-MS were significantly different from those obtained by SEC with poly(2-vinyl pyridine) molecular weight standards. The combination of the two techniques highlights the limitations of each method when done without the other.

The oil-binding capacity of chitosan was studied using the developed methods for chitosan. PLS was able to successfully model the oil-binding of chitosan indicating that multi-technique approach to polymer characterization can give reliable data that can be used to predict other properties with higher figures of merit.

Liquid chromatography with electrospray ionization mass spectrometry (LC-ESI-MS) was effectively used to determine the molecular weight distribution of synthesized aminopropylsiloxane oligomers. Single homologue siloxane standards were prepared by fractionating the sample in an octadecyl column by ion pair chromatography. The molar concentration of a siloxane homologue in each collected fraction was assigned using induced coupled plasma – optical emission spectroscopy (ICP-OES). It was shown here that multi-technique approach allows the analysis of complex polymers.

Liquid chromatography was coupled offline to MALDI-MS to study two surfactant mixes. The components of the surfactant mixes are all PEG based and are present at almost the same MW. The PEG based components only varied in their end groups. Reverse-phase chromatography with C18 stationary phase was used to separate the components in the mixture. Spectral interpretation was done along with retention time information to get more knowledge as to the correct structure of the species present in the mixture.

References

1. ECHA, *Guidance for the implementation of REACH: Guidance for monomers and polymers.*, 2008.
2. Stevens, M., *Polymer Chemistry: An Introduction*. 1990, New York: Oxford University Press.
3. *Registration, Evaluation, Authorisation and Restriction of Chemicals (REACH)*, in *EC No. 1907*, T.E.P.a.t.C.o.t.E. Union, Editor 2006,
4. Montaudo, G., F. Samperi, and M.S. Montaudo, *Characterization of synthetic polymers by MALDI-MS*. *Progress in Polymer Science*, 2006. **31**(3): p. 277-357.
5. Lavine, B.K., *Chemometrics*. *Analytical Chemistry*, 2000. **72**(12): p. 91-98.
6. Wold, S., M. Sjöström, and L. Eriksson, *PLS-regression: a basic tool of chemometrics*. *Chemometrics and Intelligent Laboratory Systems*, 2001. **58**(2): p. 109-130.
7. Aranaz, I., et al., *Functional Characterization of Chitin and Chitosan*. *Current Chemical Biology*, 2009. **3**(2): p. 203-230.
8. Kumar, M.N., et al., *Chitosan chemistry and pharmaceutical perspectives*. *Chemical Reviews*, 2004. **104**(12): p. 6017-84.
9. Kasaaï, M.R., *Various Methods for Determination of the Degree of N-Acetylation of Chitin and Chitosan: A Review*. *Journal of Agricultural and Food Chemistry*, 2009. **57**(5): p. 1667-1676.
10. Aiba, S.-i., *Studies on chitosan: 4. Lysozymic hydrolysis of partially N-acetylated chitosans*. *International Journal of Biological Macromolecules*, 1992. **14**(4): p. 225-228.
11. Bernhard, M., et al., *Robust molecular weight determination of chitosan and low-molecular chitosan oligosaccharide by size exclusion chromatography*. submitted to TrAC, *Trends Anal. Chem.*
12. Wang, W., et al., *Determination of the Mark-Houwink equation for chitosans with different degrees of deacetylation*. *International Journal of Biological Macromolecules*, 1991. **13**(5): p. 281-285.
13. Wang, W. and D. Xu, *Viscosity and flow properties of concentrated solutions of chitosan with different degrees of deacetylation*. *International Journal of Biological Macromolecules*, 1994. **16**(3): p. 149-152.
14. Qin, C., et al., *Water-solubility of chitosan and its antimicrobial activity*. *Carbohydrate Polymers*, 2006. **63**(3): p. 367-374.

15. Sannan, T., K. Kurita, and Y. Iwakura, *Studies on chitin, 2. Effect of deacetylation on solubility*. Die Makromolekulare Chemie, 1976. **177**(12): p. 3589-3600.
16. Vårum, K.M., M.H. Ottøy, and O. Smidsrød, *Water-solubility of partially N-acetylated chitosans as a function of pH: effect of chemical composition and depolymerisation*. Carbohydrate Polymers, 1994. **25**(2): p. 65-70.
17. Schatz, C., et al., *Typical Physicochemical Behaviors of Chitosan in Aqueous Solution*. Biomacromolecules, 2003. **4**(3): p. 641-648.
18. Morris, G.A., et al., *Macromolecular conformation of chitosan in dilute solution: A new global hydrodynamic approach*. Carbohydrate Polymers, 2009. **76**(4): p. 616-621.
19. Muzzarelli, R.A.A., *10.06 - Nanochitins and Nanochitosans, Paving the Way to Eco-Friendly and Energy-Saving Exploitation of Marine Resources*, in *Polymer Science: A Comprehensive Reference*, M. Editors-in-Chief: Krzysztof and M. Martin, Editors. 2012, Elsevier: Amsterdam. p. 153-164.
20. Woodgate, D.E. and J.A. Conquer, *Effects of a Stimulant-Free Dietary Supplement on Body Weight and Fat Loss in Obese Adults: A Six-Week Exploratory Study*. Current Therapeutic Research, 2003. **64**(4): p. 248-262.
21. Bokura, H. and S. Kobayashi, *Chitosan decreases total cholesterol in women: a randomized, double-blind, placebo-controlled trial*. European Journal of Clinical Nutrition, 2003. **57**(5): p. 721-725.
22. Maezaki, Y., et al., *Hypocholesterolemic Effect of Chitosan in Adult Males*. Bioscience, Biotechnology and Biochemistry, 1993. **57**(9): p. 1439-1444.
23. Gallaher, C.M., et al., *Cholesterol Reduction by Glucomannan and Chitosan Is Mediated by Changes in Cholesterol Absorption and Bile Acid and Fat Excretion in Rats*. The Journal of Nutrition, 2000. **130**(11): p. 2753-2759.
24. Liu, J., J. Zhang, and W. Xia, *Hypocholesterolaemic effects of different chitosan samples in vitro and in vivo*. Food Chemistry, 2008. **107**(1): p. 419-425.
25. Deuchi, K., et al., *Effect of the viscosity or deacetylation degree of chitosan on fecal fat excreted from rats fed on a high-fat diet*. Bioscience, Biotechnology and Biochemistry, 1995. **59**(5): p. 781-785.
26. Deuchi, K., O. Kanauchi, and E. Kobayashi, *Decreasing effect of chitosan on the apparent fat digestibility by rats fed on a high-fat diet*. Bioscience, Biotechnology and Biochemistry, 1994. **58**9: p. 1616-1613.

27. Han, L.K., Y. Kimura, and H. Okuda, *Reduction in fat storage during chitin-chitosan treatment in mice fed a high-fat diet*. International Journal of Obesity, 1999. **23**: p. 174-179.
28. Kanauchi, O., et al., *Mechanism for the inhibition of fat digestion by chitosan and for the synergistic effect of ascorbate*. Bioscience, Biotechnology and Biochemistry, 1995. **59**(5): p. 786-790.
29. Zhou, K., et al., *In vitro binding of bile acids and triglycerides by selected chitosan preparations and their physico-chemical properties*. LWT - Food Science and Technology, 2006. **39**(10): p. 1087-1092.
30. Cho, Y.I., H.K. No, and S.P. Meyers, *Physicochemical Characteristics and Functional Properties of Various Commercial Chitin and Chitosan Products*. J. Agric. Food Chem., 1998. **46**(9): p. 3839-3843.
31. No, H.K., et al., *Comparison of Physicochemical, Binding, and Antibacterial Properties of Chitosans Prepared without and with Deproteinization Process*. J. Agric. Food Chem., 2003. **51**(26): p. 7659-7663.
32. Brugnerotto, J., et al., *An infrared investigation in relation with chitin and chitosan characterization*. Polymer, 2001. **42**(8): p. 3569-3580.
33. Shigemasa, Y., et al., *Evaluation of different absorbance ratios from infrared spectroscopy for analyzing the degree of deacetylation in chitin*. International Journal of Biological Macromolecules, 1996. **18**(3): p. 237-242.
34. Bjorn-Helge, M. and R. Wehrens, *The pls package: principal component and partial least squares regression in R*. Journal of Statistical Software, 2007. **18**(2): p. 1-24.
35. Vandeginste, B.G.M., et al., *Handbook of Chemometrics and Qualimetrics: Part B. Data Handling in Science and Technology*. 1998: Elsevier.
36. Massart, D.L., et al., *Handbook of Chemometrics and Qualimetrics: Part A. Data Handling in Science and Technology*. 1998: Elsevier.
37. Parra-Barraza, H., et al., *Chitosan-Cholesterol and Chitosan-Stearic Acid Interactions at the Air-Water Interface*. Biomacromolecules, 2005. **6**(5): p. 2416-2426.
38. Schulz, P.C., et al., *Emulsification properties of chitosan*. Colloid & Polymer Science, 1998. **276**(12): p. 1159-1165.
39. Payet, L. and E.M. Terentjev, *Emulsification and Stabilization Mechanisms of O/W Emulsions in the Presence of Chitosan*. Langmuir, 2008. **24**(21): p. 12247-12252.

40. Muzzarelli, R.A.A., et al., *Chitosan taurocholate capacity to bind lipids and to undergo enzymatic hydrolysis: An in vitro model*. Carbohydrate Polymers, 2006. **66**(3): p. 363-371.
41. Thongngam, M. and D.J. McClements, *Characterization of Interactions between Chitosan and an Anionic Surfactant*. J. Agric. Food Chem., 2004. **52**(4): p. 987-991.
42. Wydro, P., B. Krajewska, and K. Hąc-Wydro, *Chitosan as a Lipid Binder: A Langmuir Monolayer Study of Chitosan–Lipid Interactions*. Biomacromolecules, 2007. **8**(8): p. 2611-2617.
43. Muzzarelli, R.A.A., et al., *Interactions of chitin, chitosan, N-lauryl chitosan and N-dimethylaminopropyl chitosan with olive oil*. Carbohydrate Polymers, 2000. **43**(3): p. 263-268.
44. Lee, D., S. Rumbelow, and S.K.R. Williams, *Identification and quantitation of trace impurities in fatty alcohol ethoxylates using HPLC and MALDI-TOF mass spectrometry*. Analytica Chimica Acta, 2009. **654**(1): p. 59-63.